DD^* potentials in chiral effective field theory and possible molecular states

Hao Xu,[1,2,3] Bo Wang,[1,2,4,5] Zhan-Wei Liu,[1,2,*] and Xiang Liu[1,2,†]

[1]School of Physical Science and Technology, Lanzhou University, Lanzhou 730000, China
[2]Research Center for Hadron and CSR Physics, Lanzhou University & Institute of Modern Physics of CAS, Lanzhou 730000, China
[3]Department of Applied Physics, School of Science, Northwestern Polytechnical University, Xian 710129, China
[4]School of Physics and State Key Laboratory of Nuclear Physics and Technology, Peking University, Beijing 100871, China
[5]Center of High Energy Physics, Peking University, Beijing 100871, China

(Received 28 August 2017; revised manuscript received 11 December 2018; published 17 January 2019)

The DD^* potentials are studied within the framework of heavy meson chiral effective field theory. We obtain the effective potentials of the DD^* system up to $O(\epsilon^2)$ at the one-loop level. In addition to the one-pion exchange contribution, the contact and two-pion exchange interactions are also investigated in detail. Furthermore, we search for the possible molecular states by solving the Schrödinger equation with the potentials. We notice that the contact and two-pion exchange potentials are numerically non-negligible and important for the existence of a bound state. In our results, no bound state is found in the $I = 0$ channel within a wide range of the cutoff parameter, while there exists a bound state in the $I = 1$ channel as the cutoff is near m_ρ in our approach.

DOI: 10.1103/PhysRevD.99.014027

I. INTRODUCTION

Chiral effective field theory (ChEFT) is an effective field theory respecting the chiral symmetry of quantum chromodynamics (QCD) at low momenta. A prominent feature of ChEFT is that the results are expanded as a power series of small momenta rather than small coupling constants, which enables us to systematically study the nonperturbative regime of the strong interaction. Pseudo-Goldstone bosons, such as pions and kaons with light masses, play very important roles in the low-energy processes. Chiral symmetry constrains the form of the interaction quite strongly. Owing to the clear power-counting scheme, ChEFT is a very powerful tool for investigating the properties of light pseudoscalar bosons [1–3].

The situation becomes complicated when heavy hadrons are involved. The power-counting rule is broken because of the large hadron masses. However, for a system with a single heavy hadron and a few light pseudoscalar bosons, the power-counting scheme can be easily rebuilt, and many approaches of ChEFT have been developed to deal with the relevant scatterings, interactions, electromagnetic moments, and other properties of such a system. Heavy hadron chiral perturbation theory, infrared regularization, and the extended-on-mass-shell scheme are frequently used in the single-heavy-hadron sector [4–18]. Unfortunately, these approaches cannot be directly extended to study the properties of a few heavy hadrons, like the nuclear force.

Two-nucleon interactions cause another power-counting problem. Two approximately on-shell nucleons in loop diagrams cause an extra enhancement compared to naive power counting, which prevents us from directly calculating the scattering matrix. Weinberg proposed a framework to deal with this issue [19,20]. One can first calculate an effective potential, i.e., the sum of all two-particle-irreducible (2PI) diagrams, and then iterate it (using, e.g., the Lippmann-Schwinger or Schrödinger equation) to retrieve the two-particle-reducible (2PR) contributions. Weinberg's formalism has since been extended and further developed [21–32]. For example, a unitary transformation was used to remove the energy dependence of the potential in Refs. [23,24]. The renormalization of potentials was carefully studied in Refs. [25,26,33–35]. The authors of Ref. [27] revisited the nucleon-nucleon potential up to next-to-next-to-next-to-leading order within ChEFT. In Refs. [28,29] the nucleon-antinucleon potential was investigated within ChEFT. Very recently, a covariant formalism of the N-N interaction was proposed in Ref. [30]. Three-body and even four-body nuclear forces have been systematically studied within ChEFT; see Refs. [31,32] for a

*liuzhanwei@lzu.edu.cn
†xiangliu@lzu.edu.cn

review. The application of ChEFT has definitely advanced our understanding of the nuclear force [36].

With successes in the study of the nuclear force, one may wonder whether ChEFT can help us comprehend the interactions of heavy (charmed, bottomed) meson systems. Obviously, since a heavy meson is heavier, we can make some assumptions such as the heavy-quark limit without worry, and thus heavy hadron ChEFT is even more suitable than that in the nucleon system.

The XYZ and similar exotic states have attracted a lot of interest in hadron physics, and it is well known that the interaction between heavy mesons is responsible for the strange behavior close to the threshold in charmonium and bottomonium spectra (see Ref. [37] for a review). This started with the discovery of the famous $X(3872)$, which was observed by the Belle Collaboration in the B decay process $B^{+-} \to K^{+-}\pi^+\pi^- J/\psi$ in 2003 [38]. $X(3872)$ is extremely close to the threshold of $D^0\bar{D}^{*0}$. Its mass is much smaller than quark model predictions (such as the Godfrey-Isgur model [39]) if it is regarded as $\chi'_{c1}(2P)$ charmonium, and moreover it has a large decay width for the isospin violation process $X(3872) \to J/\psi\rho$. After that, more XYZ and other exotic state candidates were discovered, such as the recently observed pentaquarks $P_c(4380)^+$ and $P_c(4450)^+$ [40] and the still debated $X(5568)$ [41].

There are many models dealing with these states, such as the one-boson-exchange molecular model, some underlying multiquark models, the kinematical effect, and so on (see Ref. [37] for a review). For example, in Refs. [42,43] the $D^*_{(s)}\bar{D}^*_{(s)}$ and $D\bar{D}^*$ systems were studied within the local hidden gauge formalism to dynamically generate $Y(3940)$, $Z(3930)$, $X(4160)$, and $Z_c(3900)$. In Ref. [44], the $D\bar{D}^*$ system and its relation to $Z_c(3900)$ were investigated using the covariant spectator theory. $Z_c(3900)$ was also studied using the pole-counting rule [45]. The authors of Ref. [46] discussed $D^{(*)}\bar{D}^{(*)}$ using constituent quark models, and solved the four-body Schrödinger equation with the Gaussian expansion method. The contact interaction of $D\bar{D}^*(B\bar{B}^*)$ was investigated in Ref. [47] using effective field theory, which was implemented with the heavy quark symmetry. The $D\bar{D}^*$ system was also intensively studied with different kinds of effective field theories; see Refs. [48–58] and many other works cited therein. For example, in Ref. [48] the $D\bar{D}^*$ system was studied with X effective field theory using perturbative pions. In Ref. [50], $X(3872)$ and $D\bar{D}^*$ were studied using nonperturbative pions. Moreover, the authors of Ref. [58] further included the effects of the D^* width. The study of hadronic molecules with effective field theories was reviewed in Ref. [59].

As mentioned above, there are many models dealing with heavy meson systems. Among them, the one-boson-exchange model has been used to interpret many exotic phenomena and make predictions that have been verified by later experimental discoveries of new particles. This model can provide the dynamical potentials of hadron systems, and then one can solve the Schrödinger equation to see if there is a bound state. The model has been widely used to study the interaction of two-heavy-hadron systems and related exotic states. The study of the charmed-anticharmed system and $X(3872)$ has a long history. It started with the study of pion and σ exchanges in Ref. [60], was directly extended to the multistate exchanges [61], and then included more complicated effects from S-D mixing [62], isospin violation [63], and so on. After the development of the boson exchange model (see the discussion in Ref. [64]), ChEFT was used to study the nuclear force, which helped to develop our current understanding of these phenomena. Following this trend, it is natural to use ChEFT to study heavy meson systems.

There have been many studies of heavy meson systems using the one-boson-exchange model and effective field theories, as mentioned above. Here, we investigate their higher-order effects in chiral effective field theory; we then discuss the potential in coordinate space and search for the bound state by solving the Schrödinger equation. We also compare our results with the one-boson-exchange model.

In this work, we focus on the doubly charmed-meson system DD^*, which is clearer than the hidden charmed system due to the absence of annihilation channels. It provides us with another way to understand heavy-flavor dynamics and nonperturbative QCD. Furthermore, it is analogous to the deuteron since they both have contact, one-pion exchange (OPE), and two-pion exchange (TPE) contributions without annihilation channels in our framework.

Currently, the only observed doubly heavy-flavor system is the Ξ_{cc}^{++} baryon, which was first discovered by the SELEX Collaboration [65]. Systems like ccu and ccd have been discussed a lot, and their properties (such as masses and electromagnetic moments) require further clarification [66–73]. Very recently, the LHCb Collaboration confirmed the existence of Ξ_{cc}^{++} but disfavored the mass measured at SELEX [74]. Using current techniques and experiments it is also possible to search for the doubly charmed boson made of DD^*.

The $D^{(*)}D^{(*)}(B^{(*)}B^{(*)})$ system was studied in Ref. [75] to search for bound and resonant states, and they used pion and vector-meson exchange potentials which are constrained by heavy quark symmetry and chiral symmetry. They found that in the isospin-0 channel there exists a bound state in the S wave with a binding energy of 62.3 MeV, but no bound state was found in the S-wave isospin-1 channel. The $D^{(*)}D^{(*)}$ system was studied in Ref. [76] using the one-boson-exchange model, and it was found that there exists a bound state consisting of DD^* with a binding energy of 5–43 MeV in the isospin-0 channel. The authors of Ref. [77] investigated deuteron-like molecules with both open charm and bottom using heavy-meson

effective theory. In Ref. [78], charm-beauty meson bound states were dynamically generated from the $B^{(*)}D^{(*)}$ and $B^{(*)}\bar{D}^{(*)}$ interactions and their scattering lengths were obtained. There have also been lattice studies of BB and BB^* interactions [79–81]. In particular, the authors of Ref. [81] considered both diquark-antidiquark and meson-meson configurations. In Ref. [82], we investigated the $\bar{B}\bar{B}$ interaction within heavy meson chiral effective field theory (HMChEFT). We obtained the potentials of the $\bar{B}\bar{B}$ system at the one-loop level, and discussed the contact and two-pion exchange contributions in momentum space.

In this work we investigate the DD^* system. As we mentioned before, we need to study the potentials first, and then we can indirectly access the physical observables. Furthermore, the potential in coordinate space can give us more intuitive information about interactions between mesons, and we can further solve a dynamic equation to see whether there exists a hadronic molecule. This paper is organized as follows. After this Introduction, we elucidate the framework in Secs. II and III. In Sec. IV, we give the results for the potentials in momentum space. In Sec. V, we study the potentials in coordinate space to search for possible molecules. Finally, in Sec. VI we summarize and present our conclusions.

II. LAGRANGIANS AND THE WEINBERG SCHEME

To study the DD^* system using HMChEFT, we need to derive the Lagrangians and provide results systematically in a strict power-counting scheme. Our results are arranged order by order with the small parameter $\epsilon = p/\Lambda_\chi$, where p can be the momentum of a pion, the residual momentum of heavy mesons, or the D-D^* mass splitting, and Λ_χ represents either the chiral symmetry breaking scale or the mass of the heavy mesons. In this work, flavor SU(2) symmetry is always assumed.

A. Lagrangians at the leading order

At the leading order $O(\epsilon^0)$, both OPE diagrams and contact diagrams contribute to the amplitudes, and thus we should first build the Lagrangians for $DD^*\pi$ interaction vertices, the corresponding contact vertices, and so on.

The $DD^*\pi$ Lagrangian at leading order [83–85] is given by

$$\mathcal{L}^{(1)}_{H\phi} = -\langle (iv\cdot\partial H)\bar{H}\rangle + \langle Hv\cdot\Gamma\bar{H}\rangle + g\langle H\not{u}\gamma_5\bar{H}\rangle - \frac{1}{8}\delta\langle H\sigma^{\mu\nu}\bar{H}\sigma_{\mu\nu}\rangle. \quad (1)$$

In the above, the H field represents the (D, D^*) doublet in the heavy-quark limit,

$$H = \frac{1+\not{v}}{2}(P^*_\mu\gamma^\mu + iP\gamma_5),$$
$$\bar{H} = \gamma^0 H^\dagger\gamma^0 = (P^{*\dagger}_\mu\gamma^\mu + iP^\dagger\gamma_5)\frac{1+\not{v}}{2},$$
$$P = (D^0, D^+), \qquad P^*_\mu = (D^{*0}, D^{*+})_\mu. \quad (2)$$

$v = (1,0,0,0)$ stands for the 4-velocity of the H field. The last term in Eq. (1) is included to account for the D-D^* mass shift which is not zero in the chiral limit, and δ is the mass difference in the (D, D^*) doublet. The axial-vector field u and chiral connection Γ are expressed as

$$\Gamma_\mu = \frac{i}{2}[\xi^\dagger, \partial_\mu\xi], \qquad u_\mu = \frac{i}{2}\{\xi^\dagger, \partial_\mu\xi\}, \quad (3)$$

where $\xi = \exp(i\phi/2f)$, f is the bare constant for pion decay, and

$$\phi = \sqrt{2}\begin{pmatrix} \frac{\pi^0}{\sqrt{2}} & \pi^+ \\ \pi^- & -\frac{\pi^0}{\sqrt{2}} \end{pmatrix}. \quad (4)$$

The contact Lagrangian at $O(\epsilon^0)$ is constructed as follows [47,51,82]:

$$\begin{aligned}\mathcal{L}^{(0)}_{4H} = {} & D_a\mathrm{Tr}[H\gamma_\mu\bar{H}]\mathrm{Tr}[H\gamma^\mu\bar{H}] \\ & + D_b\mathrm{Tr}[H\gamma_\mu\gamma_5\bar{H}]\mathrm{Tr}[H\gamma^\mu\gamma_5\bar{H}] \\ & + E_a\mathrm{Tr}[H\gamma_\mu\tau^a\bar{H}]\mathrm{Tr}[H\gamma^\mu\tau_a\bar{H}] \\ & + E_b\mathrm{Tr}[H\gamma_\mu\gamma_5\tau^a\bar{H}]\mathrm{Tr}[H\gamma^\mu\gamma_5\tau_a\bar{H}], \end{aligned} \quad (5)$$

where D_a, D_b, E_a, and E_b are four independent low-energy constants (LECs).

B. Lagrangians at the next-to-leading order

At chiral order $O(\epsilon^2)$, the amplitudes consist of the contact corrections, OPE corrections, and TPE amplitudes. These one-loop amplitudes must be renormalized with the help of $O(\epsilon^2)$ Lagrangians. The divergences in the one-loop amplitudes are canceled by the infinite parts of the LECs in the following Lagrangians [82]:

$$\begin{aligned}\mathcal{L}^{(2,h)}_{4H} = {} & D^h_a\mathrm{Tr}[H\gamma_\mu\bar{H}]\mathrm{Tr}[H\gamma^\mu\bar{H}]\mathrm{Tr}(\chi_+) \\ & + D^h_b\mathrm{Tr}[H\gamma_\mu\gamma_5\bar{H}]\mathrm{Tr}[H\gamma^\mu\gamma_5\bar{H}]\mathrm{Tr}(\chi_+) \\ & + E^h_a\mathrm{Tr}[H\gamma_\mu\tau^a\bar{H}]\mathrm{Tr}[H\gamma^\mu\tau_a\bar{H}]\mathrm{Tr}(\chi_+) \\ & + E^h_b\mathrm{Tr}[H\gamma_\mu\gamma_5\tau^a\bar{H}]\mathrm{Tr}[H\gamma^\mu\gamma_5\tau_a\bar{H}]\mathrm{Tr}(\chi_+), \end{aligned} \quad (6)$$

$$\begin{aligned}\mathcal{L}_{4H}^{(2,v)} =& \{D_{a1}^{v}\mathrm{Tr}[(v\cdot DH)\gamma_\mu(v\cdot D\bar{H})]\mathrm{Tr}[H\gamma^\mu\bar{H}]\\ &+D_{a2}^{v}\mathrm{Tr}[(v\cdot DH)\gamma_\mu\bar{H}]\mathrm{Tr}[(v\cdot DH)\gamma^\mu\bar{H}]\\ &+D_{a3}^{v}\mathrm{Tr}[(v\cdot DH)\gamma_\mu\bar{H}]\mathrm{Tr}[H\gamma^\mu(v\cdot D\bar{H})]\\ &+D_{a4}^{v}\mathrm{Tr}[((v\cdot D)^2H)\gamma_\mu\bar{H}]\mathrm{Tr}[H\gamma^\mu\bar{H}]\\ &+D_{b1}^{v}\mathrm{Tr}[(v\cdot DH)\gamma_\mu\gamma_5(v\cdot D\bar{H})]\mathrm{Tr}[H\gamma^\mu\gamma_5\bar{H}]+\cdots\\ &+E_{a1}^{v}\mathrm{Tr}[(v\cdot DH)\gamma_\mu\tau^a(v\cdot D\bar{H})]\mathrm{Tr}[H\gamma^\mu\tau_a\bar{H}]+\cdots\\ &+E_{b1}^{v}\mathrm{Tr}[(v\cdot DH)\gamma_\mu\gamma_5\tau^a(v\cdot D\bar{H})]\mathrm{Tr}[H\gamma^\mu\gamma_5\tau_a\bar{H}]\\ &+\cdots\}+\mathrm{H.c.}, \end{aligned} \tag{7}$$

$$\begin{aligned}\mathcal{L}_{4H}^{(2,q)} =& \{D_{1}^{q}\mathrm{Tr}[(D^\mu H)\gamma_\mu\gamma_5(D^\nu\bar{H})]\mathrm{Tr}[H\gamma_\nu\gamma_5\bar{H}]\\ &+D_{2}^{q}\mathrm{Tr}[(D^\mu H)\gamma_\mu\gamma_5\bar{H}]\mathrm{Tr}[(D^\nu H)\gamma_\nu\gamma_5\bar{H}]\\ &+D_{3}^{q}\mathrm{Tr}[(D^\mu H)\gamma_\mu\gamma_5\bar{H}]\mathrm{Tr}[H\gamma_\nu\gamma_5(D^\nu\bar{H})]\\ &+D_{4}^{q}\mathrm{Tr}[(D^\mu D^\nu H)\gamma_\mu\gamma_5\bar{H}]\mathrm{Tr}[H\gamma_\nu\gamma_5\bar{H}]\\ &+E_{1}^{q}\mathrm{Tr}[(D^\mu H)\gamma_\mu\gamma_5\tau^a(D^\nu\bar{H})]\mathrm{Tr}[H\gamma_\nu\gamma_5\tau_a\bar{H}]\\ &+\cdots\}+\mathrm{H.c.},\ldots, \end{aligned} \tag{8}$$

where

$$\begin{aligned}\tilde{\chi}_\pm &= \chi_\pm-\frac{1}{2}\mathrm{Tr}[\chi_\pm],\\ \chi_\pm &= \xi^\dagger\chi\xi^\dagger\pm\xi\chi\xi,\\ \chi &= m_\pi^2. \end{aligned} \tag{9}$$

Note that the term $\mathcal{L}_{4H}^{(2,d)}$ in Ref. [82] vanishes in our SU(2) case.

In addition to canceling the divergences of the loop diagrams, the above Lagrangians also contain finite parts that contribute to tree-level diagrams at $O(\epsilon^2)$. They are governed by the large number of LECs appearing in Eqs. (6)–(8).

C. Weinberg scheme

In this work, we adopt Weinberg's power-counting scheme to study the DD^* systems [19,20]. This framework has been widely applied to nucleon-nucleon systems, as mentioned in the Introduction. Let us start with a nucleon-nucleon TPE box diagram, depicted in Fig. 1. As illustrated in Ref. [82], the amplitude can be written using the heavy hadron formalism:

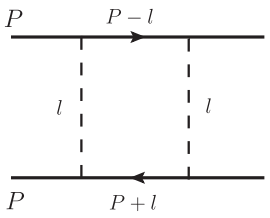

FIG. 1. A typical TPE box diagram of the nucleon-nucleon interaction. The solid line stands for the nucleon and the dashed line stands for the pion.

$$\begin{aligned} & i\int d^4l\frac{i}{l^0+P^0-\frac{\vec{q}_1^{\,2}}{2M_N}+i\varepsilon}\frac{i}{-l^0+P^0-\frac{\vec{q}_2^{\,2}}{2M_N}+i\varepsilon}\times\cdots\\ &= i\int d^3l\int dl^0\frac{i}{l^0+P^0-\frac{\vec{q}_1^{\,2}}{2M_N}+i\varepsilon}\frac{i}{-l^0+P^0-\frac{\vec{q}_2^{\,2}}{2M_N}+i\varepsilon}\\ &\quad\times\cdots\\ &= \int d^3l\frac{\pi}{P^0-\frac{1}{2}\left(\frac{\vec{q}_1^{\,2}}{2M_N}+\frac{\vec{q}_2^{\,2}}{2M_N}\right)+i\varepsilon}\cdots\\ &= \int d^3l\frac{\pi}{\frac{\vec{P}^2}{(2M_N)}-\frac{1}{2}\left(\frac{\vec{q}_1^{\,2}}{2M_N}+\frac{\vec{q}_2^{\,2}}{2M_N}\right)+i\varepsilon}\cdots\\ &= -\int d^3l\frac{\pi}{\frac{\vec{l}^{\,2}}{(2M_N)}+i\varepsilon}\cdots, \end{aligned} \tag{10}$$

where m_N is the mass of the nucleon, $\vec{q}_1=\vec{P}+\vec{l}$, and $\vec{q}_2=\vec{P}-\vec{l}$. Naive power counting gives the l^0 integral $O(|\vec{P}|^{-1})$, while we notice from Eq. (10) that the l^0 integral should be of $O(|\vec{P}|^{-2})$, i.e., the true order is enhanced by $|\vec{P}|^{-1}$. Such an enhancement definitely violates the power-counting rule, which would invalidate the chiral expansion. As pointed out in Refs. [19,20], the origin of such a contradiction comes from the double poles in Eq. (10), which is related to the 2PR part of the box diagram in Fig. 1.

With the above analysis in mind, we find ourselves in the same situation when studying the interaction of the doubly charmed meson pair, and thus cannot directly calculate the scattering amplitude. Alternatively, we can apply Weinberg's power-counting scheme. First, with the usual power-counting rule, we compute the 2PI contributions of all diagrams, which leads to the effective potentials. Then, we substitute the potentials into iterated equations (such as the Lippmann-Schwinger or Schrödinger equation) to recover the 2PR contributions. Finally, we obtain the desired scattering amplitudes or energy levels.

III. EFFECTIVE POTENTIALS OF THE DD^* SYSTEM

The effective potentials of the DD^* system receive contributions from the contact and OPE diagrams at the leading order $O(\epsilon^0)$. At the next-to-leading order $O(\epsilon^2)$, there are both tree and one-loop corrections. The effective potentials $\mathcal{V}$ are related to the Feynman amplitudes $\mathcal{M}$ of 2PI diagrams,

$$\mathcal{V}=\frac{-1}{4}\mathcal{M}, \tag{11}$$

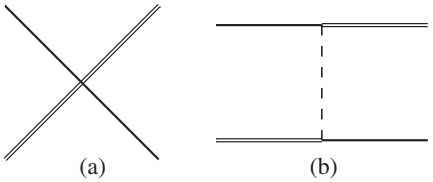

FIG. 2. Tree-level diagrams of the processes $DD^* \to DD^*$ at $O(\epsilon^0)$. The left diagram represents the contact terms, and the right one is the one-pion-exchange diagram. The solid, double-solid, and dashed lines stand for the D, D^*, and a pion, respectively.

which follows from the one-boson-exchange model (despite some differences in conventions) [86,87].

At the lowest order $O(\epsilon^0)$, there are two diagrams at tree level, as illustrated in Fig. 2. They represent the contact and OPE contributions, respectively. The contact terms mainly affect the short-range interaction between particles, while the OPE contribution determines the behavior of the long-range interaction.

With the Lagrangians (1) and (5), the corresponding amplitudes can be easily computed. For the process $D(p_1)D^*(p_2) \to D(p_3)D^*(p_4)$ with isospin $I = 1$, the amplitudes for the diagrams in Figs. 2(a) and 2(b) read

$$\mathcal{M}^{(0)}_{I=1(a)} = i(-8D_a + 8D_b - 8E_a + 8E_b)\varepsilon(p_2)\cdot\varepsilon^*(p_4), \tag{12}$$

$$\mathcal{M}^{(0)}_{I=1(b)} = i(-1)\frac{g^2}{f^2}\frac{p_\mu p_\nu}{p^2 - m^2}\varepsilon^\mu(p_2)\varepsilon^{*\nu}(p_4). \tag{13}$$

For the process $D(p_1)D^*(p_2) \to D(p_3)D^*(p_4)$ with $I = 0$, the amplitudes are

$$\mathcal{M}^{(0)}_{I=0(a)} = i(24E_a + 24E_b - 8D_a - 8D_b)\varepsilon(p_2)\cdot\varepsilon^*(p_4), \tag{14}$$

$$\mathcal{M}^{(0)}_{I=0(b)} = i(-3)\frac{g^2}{f^2}\frac{p_\mu p_\nu}{p^2 - m^2}\varepsilon^\mu(p_2)\varepsilon^{*\nu}(p_4). \tag{15}$$

In the above equations, the momentum $p = p_1 - p_4$, the superscript (0) denotes the order $O(\epsilon^0)$, and the subscripts "$I = 0$, 1" stand for the process $DD^* \to DD^*$ with isospin 0 and 1, respectively.

At $O(\epsilon^2)$, a number of diagrams emerge. The tree diagrams at $O(\epsilon^2)$ are similar to Fig. 2(a), but the vertices should be replaced with those from the Lagrangians (6)–(8). There are three additional sets of one-loop diagrams.

The diagrams in the first set are for one-loop corrections to the contact terms. They are depicted in Fig. 3. Figures 3(a1)–(a12) represent contributions from the wave-function renormalization of external legs.

We show the second set of diagrams in Fig. 4. They represent one-loop corrections to the OPE diagrams.

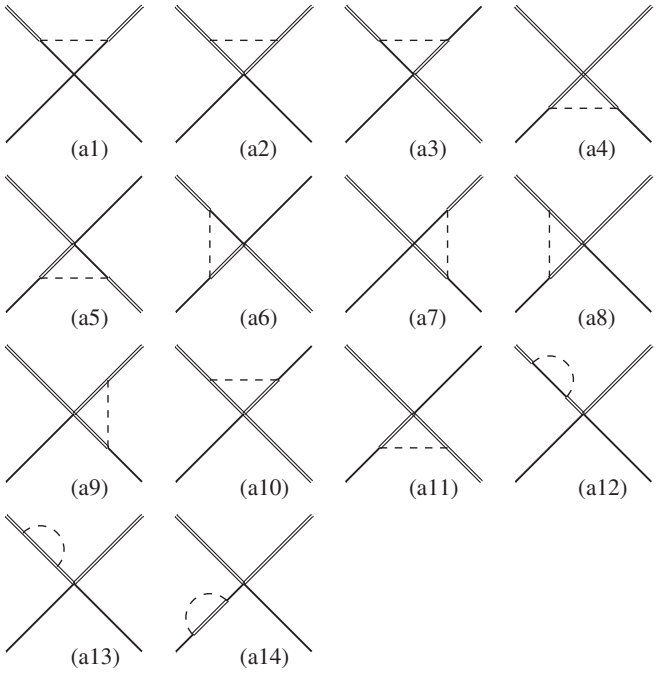

FIG. 3. One-loop corrections to the contact terms at $O(\epsilon^2)$. The solid, double-solid, and dashed lines stand for D, D^*, and a pion, respectively.

Figures 4(b1)–4(b6) and Figs. 4(b8)–4(b9) contribute to the renormalization of the $DD^*\pi$ vertex. Therefore, we must use the value for the bare coupling g in $\mathcal{M}^{(0)}$ at $O(\epsilon^0)$ to avoid double counting. We show the relation between the bare coupling g and the experimental coupling $g^{(2)}$ in Eq. (B1) in Appendix B. Similarly, the bare decay constant f should be used in Eqs. (13) and (15) as well.

The final set is for the TPE diagrams, which are shown in Fig. 5. They are important for the medium-range interaction.

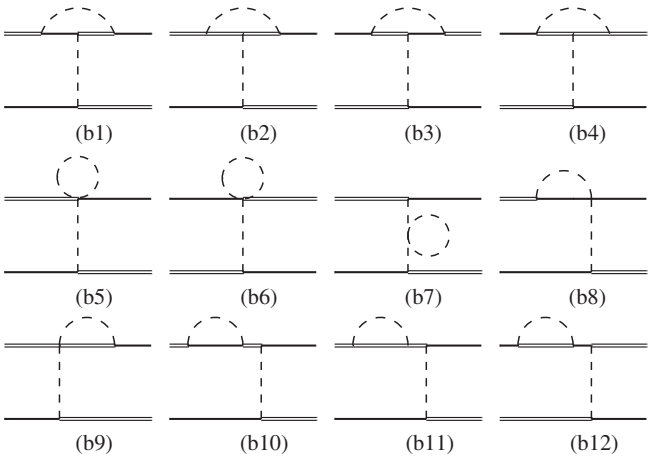

FIG. 4. One-loop corrections to the one-pion-exchange diagrams at $O(\epsilon^2)$. The solid, double-solid, and dashed lines stand for D, D^*, and a pion, respectively.

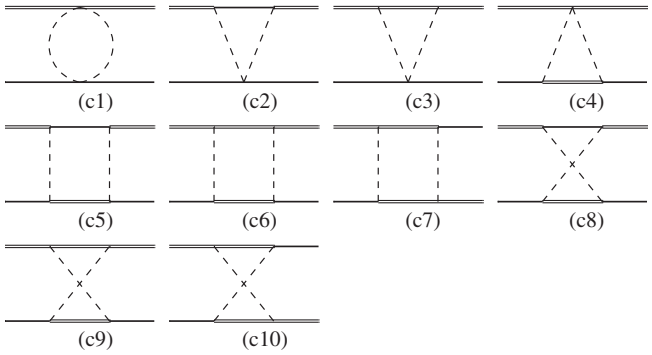

FIG. 5. Two-pion-exchange diagrams at $O(\epsilon^2)$. The solid, double-solid, and dashed lines stand for D, D^*, and a pion, respectively.

As discussed in the previous section, some diagrams (such as the box diagrams in Fig. 5) contain a 2PR part that should be subtracted. If there is a loop function of a box diagram like

$$\int d^4l \frac{1}{v\cdot l + a + i\varepsilon}\frac{1}{-v\cdot l - a + i\varepsilon}\times\cdots, \tag{16}$$

following Refs. [82,88], we can separate the 2PR and 2PI parts as

$$\begin{aligned}&\frac{1}{v\cdot l + a + i\varepsilon}\frac{1}{-v\cdot l - a + i\varepsilon}\\&\quad=\frac{1}{v\cdot l + a + i\varepsilon}\left[-\frac{1}{v\cdot l + a + i\varepsilon}+2\pi\delta(v\cdot l + a)\right].\end{aligned} \tag{17}$$

The term proportional to the Dirac δ function is just the 2PR part, which should be dropped in the potentials.

All of the one-loop amplitudes of the diagrams in Figs. 3–5 for the processes $DD^* \to DD^*$ are shown in Appendix A. The divergences of the loop functions are regularized using dimensional regularization, and subtracted using the modified minimal subtraction scheme. Also, we list the definitions of the loop functions in Appendix C. The finite parts of the high-order Lagrangians should also contribute to tree-level diagrams at $O(\epsilon^2)$, and they are governed by a large number of LECs. However, we need plenty of data for $D\bar{D}^*$ (or other channels, such as $D\bar{D}$ or DD) scattering in different partial waves to fit these LECs, but this is currently lacking. Therefore, in the present work we only focus on the loop contributions at $O(\epsilon^2)$.

We can easily obtain the potentials $\mathcal{V}_{I=1}^{DD^*}$ and $\mathcal{V}_{I=0}^{DD^*}$ from the Feynman amplitudes by multiplying by a factor $-1/4$. The polarized vectors in the potentials were dealt with delicately in Ref. [89]. In this work, we only consider the S-wave interaction, which leads to the following substitutions in Eqs. (12)–(15) and (A1)–(A33):

$$\vec{\varepsilon}(p_2)\cdot\vec{\varepsilon}^*(p_4) \rightarrowtail 1, \tag{18}$$

$$\vec{\varepsilon}(p_2)\cdot\vec{p}\vec{\varepsilon}^*(p_4)\cdot\vec{p} \rightarrowtail \frac{1}{3}\vec{p}^2, \tag{19}$$

where we follow the one-boson exchange model in Refs. [86,87]. After all of these procedures, the effective potentials $\mathcal{V}_{I=1}^{DD^*}$ and $\mathcal{V}_{I=0}^{DD^*}$ in momentum space can be obtained. However, the potentials are energy dependent. A solution to this problem was proposed in Refs. [23,24], where a unitary transformation was used to get rid of the energy dependence. In this work, we just set the transferred energies equal to zero, i.e., $p^0 = 0$ and $q^0 = 0$ for simplicity, as in the one-boson exchange model [60]. Also, we set the residual energies of the heavy mesons equal to zero.

IV. NUMERICAL RESULTS OF POTENTIALS IN MOMENTUM SPACE

We use the following input parameters to obtain the numerical results: $m_\pi = 0.139$ GeV, the mass difference $\delta = 0.142$ GeV, $f_\pi = 0.086$ GeV, and the renormalization scale $\mu = 4\pi f$. Many methods have been used to investigate the constant for $D^{(*)}D^{(*)}\pi$ coupling, such as the lattice studies [90–92], QCD sum rules [93–97], and other approaches [98–100]. The experimental process $D^* \to D\pi$ was fit to obtain the renormalized coupling $g^{(2)}$ [101], and we get the bare coupling $g = 0.65$ by using the $O(\epsilon^2)$ correction in Eq. (B1).

First, we list the results for the contact contributions. For $\mathcal{V}_{I=1}^{DD^*}$ in the isospin-1 channel, the effective potentials at $O(\epsilon^0)$ and $O(\epsilon^2)$ are

$$\mathcal{V}_{I=1}^{(0)} = -2D_a + 2D_b - 2E_a + 2E_b, \tag{20}$$

$$\begin{aligned}\mathcal{V}_{I=1}^{(2)} =& -(0.253 + 0.031i)D_b + 0.044E_a\\&- (0.166 + 0.030i)E_b.\end{aligned} \tag{21}$$

For the isospin-0 channel, we obtain

$$\mathcal{V}_{I=0}^{(0)} = -2D_a - 2D_b + 6E_a + 6E_b, \tag{22}$$

$$\begin{aligned}\mathcal{V}_{I=0}^{(2)} =& -(1.214 + 0.190i)E_a + (0.116 + 0.047i)D_b\\&+ (0.025 - 0.143i)E_b.\end{aligned} \tag{23}$$

Obviously, the contact contributions are just constants, and they result in $\delta(r)$ potentials in coordinate space, which describes the short-distance effect. From Eqs. (20)–(23), we see that the convergence of the series expansion is good. From Eqs. (21) and (23), the contact coupling constant D_a does not appear in the effective potential at $O(\epsilon^2)$ because the contributions from the D_a term are canceled among the various diagrams in Fig. 3.

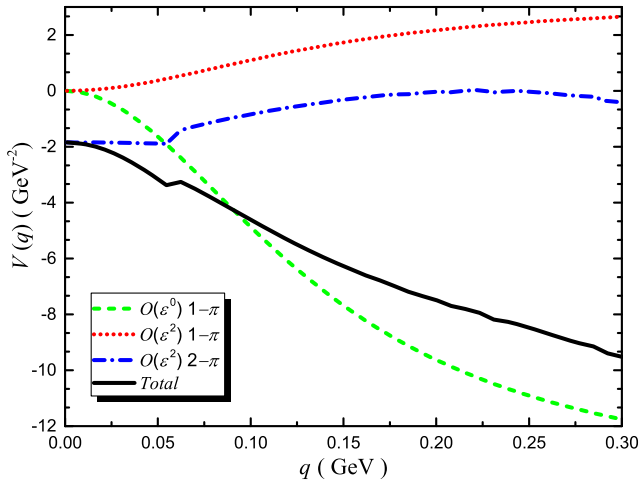

FIG. 6. OPE and TPE potentials $\mathcal{V}^{DD^*}_{I=0}$ for the isospin-0 channel. q stands for the 3-momentum in units of GeV, and the y axis represents the effective potential in units of GeV^{-2}. The red dotted and green dashed lines describe the OPE potentials at the leading and next-to-leading order, individually. The blue dot-dashed line is for the TPE potential. The sum of the three contributions is represented by the black solid line.

Next, we focus on the properties of the OPE and TPE contributions. We illustrate the corresponding potentials for channels with isospin 0 and 1 in Figs. 6 and 7, respectively, ranging from $q = |\mathbf{q}| = 0$ to 300 MeV.

From Figs. 6 and 7, one can see that the OPE contributions at $O(\epsilon^0)$ are dominant in both the $I = 0$ and $I = 1$ channels since the green dashed lines are close to the black solid ones. The OPE potentials at $O(\epsilon^2)$ are small compared to those at $O(\epsilon^0)$. The sums of the OPE contributions are negative in Figs. 6 and 7, which means the OPE interaction is attractive in both the $I = 0$ and $I = 1$ channel. We also notice that the OPE interaction for $I = 0$ is more attractive than for $I = 1$.

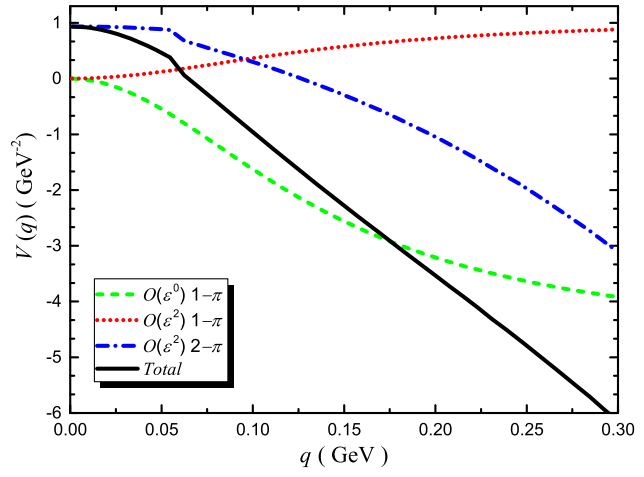

FIG. 7. OPE and TPE potentials $\mathcal{V}^{DD^*}_{I=1}$. The line types and color schemes match those of Fig. 6.

The situation for the TPE potentials is more complicated. The TPE contributions behave differently in the $I = 0$ and $I = 1$ channels. In Fig. 6, the TPE interaction for the $I = 0$ channel is attractive in the range 0–300 MeV, and it tends to grow beyond 300 MeV. The TPE potential at $O(\epsilon^2)$ is larger than the OPE one at $O(\epsilon^0)$ in the range 0–60 MeV, while the OPE contribution rapidly exceeds that of TPE when q is larger than 60 MeV, and becomes dominant. We can say that the convergence of the chiral series is good. Looking at Fig. 7, we see that the TPE potential is repulsive in the range 0–120 MeV, while it becomes attractive as q increases beyond the range. The TPE potential at $O(\epsilon^2)$ is smaller than the OPE contribution at $O(\epsilon^0)$ in the lower range of the momentum, and becomes comparable for large momenta. This seems to indicate that the convergence of the chiral series would be spoiled at larger transferred momenta. From the blue dot-dashed lines in Figs. 6 and 7, we see that the TPE interaction for $I = 1$ is more attractive than that for $I = 0$.

Let us turn to the sum of these three contributions. The total contribution in Fig. 6 for $\mathcal{V}^{DD^*}_{I=0}$ is attractive, while in Fig. 7 for $\mathcal{V}^{DD^*}_{I=1}$ it is less attractive and tends to be repulsive as q becomes smaller than 50 MeV because of the repulsive TPE contribution. This makes us wonder whether there a bound state could form in the DD^* system with the inclusion of contact contributions.

V. POTENTIALS IN COORDINATE SPACE AND POSSIBLE MOLECULAR STATES

Although the pion exchange interaction is attractive at most momenta, there can still be no bound states if it is not attractive enough. Moreover, the contact interaction might be repulsive, which would further decrease the possibility for the existence of a bound state. Thus the contact potentials must first be obtained numerically by determining the LECs. After that, we can investigate the effective potentials in coordinate space, and then solve the Schrödinger equation to search for possible molecular states.

A. Determination of LECs

We determine the LECs in the contact contributions (20)–(23) with the resonance saturation model [64,102–105]. We assume that these short-range couplings result from the ρ and ϕ exchanges as in Ref. [106], as well as other meson exchanges (scalar and axial-vector). Although it may be a rough estimate, it is meaningful to make such an attempt. The $D^{(*)}D^{(*)}V$ Lagrangian respecting heavy quark symmetry and U(2) flavor symmetry is given by [76]

$$\mathcal{L}_{HHV} = i\beta\langle Hv_\mu(V^\mu - \rho^\mu)\bar{H}\rangle + i\lambda\langle H\sigma_{\mu\nu}F^{\mu\nu}(\rho)\bar{H}\rangle. \quad (24)$$

In the above, H is the same as in Eq. (2), $F_{\mu\nu} = \partial_\mu\rho_\nu - \partial_\nu\rho_\mu - [\rho_\mu, \rho_\nu]$ with $\rho_\mu = \frac{ig_v}{\sqrt{2}}\hat{\rho}_\mu$, and the multiplet $\hat{\rho}$ is defined by

$$\hat{\rho}^{\mu} = \begin{pmatrix} \frac{\rho^0}{\sqrt{2}} + \frac{\omega}{\sqrt{2}} & \rho^+ \\ \rho^- & -\frac{\rho^0}{\sqrt{2}} + \frac{\omega}{\sqrt{2}} \end{pmatrix}^{\mu}. \tag{25}$$

The coupling constants $g_v = 5.8$, $\lambda = 0.56\ \mathrm{GeV}^{-1}$, and $\beta = 0.9$ [76]. As for the scalar exchanges S (σ, f_0, a_0), we use [76,105]

$$\mathcal{L}_{HHS} = g_{HHS}\langle HS\bar{H}\rangle, \tag{26}$$

where $g_{HHa_0(f_0)} = \sqrt{3}g_{HH\sigma}$ [105], $g_{HH\sigma} = \frac{g_\pi}{2\sqrt{6}}$, and $g_\pi = 3.73$ [107]. For the axial-vector mesons A_V (a_1, f_1), we use

$$\mathcal{L}_{HHA_V} = g_{HHA_V}\langle H\gamma_\mu\gamma_5 A_V^\mu \bar{H}\rangle. \tag{27}$$

After matching the meson exchange amplitudes to the contact amplitudes with four independent isospin channels of $D^{(*)}D^{(*)} \to D^{(*)}D^{(*)}$, we obtain

$$D_a = -\frac{\beta^2 g_v^2}{8m_\omega^2} - \frac{g_s^2}{2m_\sigma^2} - \frac{g_{s0}^2}{12m_{f_0}^2}, \qquad E_a = -\frac{\beta^2 g_v^2}{8m_\rho^2} - \frac{g_{s0}^2}{4m_{a_0}^2},$$
$$D_b = \frac{g_{HHA_V}^2}{8m_{a_1}^2}, \qquad E_b = \frac{g_{HHA_V}^2}{8m_{f_1}^2}. \tag{28}$$

However, we cannot find any inputs for the axial-vector meson coupling g_{HHA_V}, and therefore we simply assume that the low-energy constants are saturated by resonances with masses below 800 MeV. We estimate their errors with the contributions from the other four particles: f_0, a_0, f_1, and a_1. $|g_{HHA_V}|$ is set to $\beta g_v \sim 5$. We finally get the numerical values

$$D_a = -6.62 \pm 0.15, \qquad E_a = -5.74 \pm 0.45,$$
$$D_b = 0 \pm 1.96, \qquad E_b = 0 \pm 1.89. \tag{29}$$

B. Potentials in coordinate space

After the determination of the LECs, we are ready to transfer the potentials into coordinate space:

$$\mathcal{V}(\mathbf{r}) = \int \frac{d\mathbf{q}}{(2\pi)^3}\mathcal{V}(\mathbf{q})e^{i\mathbf{q}\cdot\mathbf{r}}. \tag{30}$$

However, since $\mathcal{V}(\mathbf{q})$ in ChEFT is proportional to the power series of $\mathbf{q}$, the divergence of the higher-order terms is much worse. The evaluation of $\mathcal{V}(\mathbf{r})$ is essentially a nonperturbative problem, and it originates from the resummation of the 2PI potentials. We have to regularize Eq. (30) nonperturbatively. Enormous efforts have been made to explore the nonperturbative renormalization [21,23,108–113]. Here we resort to a simple Gaussian cutoff $\exp(-\vec{p}^{2n}/\Lambda^{2n})$ to suppress the higher-momentum contributions, as in Refs. [22,24,30]. We use $n = 2$ as in Ref. [30]. In the nucleon-nucleon ChEFT, the value of the cutoff parameter is commonly below the ρ meson mass [27], and therefore we adopt $\Lambda = 0.7$ GeV in our work.

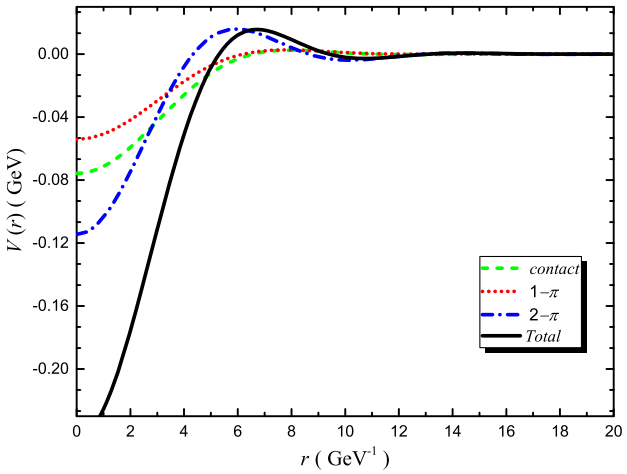

FIG. 8. S-wave potentials of the DD^* system with $I = 0$ in units of GeV. The green dashed, red dotted, and blue dot-dashed lines stand for the contact, OPE, and TPE contributions, respectively. The full potential is shown by the black solid line.

The resulting full potentials are shown in Figs. 8 and 9, where we set $\Lambda = 0.7$ GeV. From Figs. 8 and 9, we find that the OPE and TPE interactions are attractive in both cases, and the contact terms lead to an attractive interaction in the $I = 0$ channel and a repulsive interaction in the $I = 1$ channel. Obviously, this difference increases the possibility for a bound state to form in the $I = 0$ channel rather than in the $I = 1$ channel. Let us focus on the total results. The total short-distance potential for the $I = 1$ channel is repulsive and small, while that for the $I = 0$ channel is attractive and large.

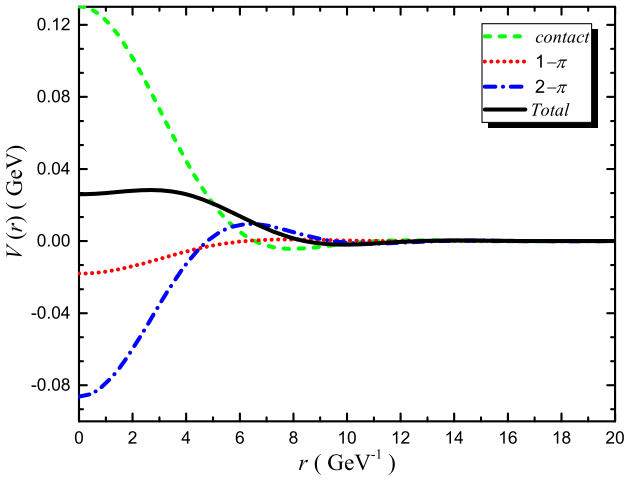

FIG. 9. S-wave potentials of the DD^* system with $I = 1$ in units of GeV. The line types and color schemes match those of Fig. 8.

C. Possible bound states

With the potentials in hand, we are finally able to solve the Schrödinger equation. We find a bound state with a binding energy around 17.5 MeV in the $I = 0$ channel, and there is no bound state in the $I = 1$ channel.

The radial wave function for the $I = 0$ channel is plotted in Fig. 10. It extends over a rather large distance, which means the constituents D and D^* are separated.

It is worth noticing that in the pion and vector-meson exchange potential model [75] a bound state was found with a binding energy of 62.3 MeV in the $I = 1$ channel, while no state was found in the $I = 1$ channel. In the one-boson exchange model, a bound state was also found in the $I = 0$ channel, with a binding energy of about 5–43 MeV and a reasonable cutoff [76]. No bound state was found in the $I = 1$ channel in that model either [76]. Our results are consistent.

From Fig. 9, we notice that the contact interaction is repulsive at short distances. However, we still cannot find a bound state even if we drop the contact interaction in the $I = 1$ channel, which implies that the pion exchange interaction is not attractive enough to bind DD^*. If we repeat these steps and turn off the contact potential in the $I = 0$ channel, the shallow bound state disappears. We also cannot obtain a reasonable energy eigenvalue of the Schrödinger equations if we keep the OPE potentials themselves for the two channels. The attractive contact and TPE interactions are important for the existence of a molecule in the $I = 0$ channel.

Theoretically, obtained observables (such as the binding energy) are independent of the regularization procedure in Eq. (30). The formal dependence on the cutoff Λ in Eq. (30) can be compensated by the Λ dependence of the LECs. However, in practice the results are sometimes sensitive to different choices of Λ. Here we investigate the influence of the cutoff with the LECs fixed. We plot the full potentials with different cutoffs in Fig. 11. From the figure, we notice that the potential becomes deeper and steeper for short distances as the cutoff increases. After solving the Schrödinger equation, we obtain binding energies of 1.1, 17.5, and 53.1 MeV with $\Lambda = 0.6$ GeV, 0.7 GeV, and m_ρ, respectively. The binding energy is sensitive to the cutoff. However, a bound-state solution exists as the cutoff is near m_ρ. Furthermore, as we stressed earlier, the cutoff dependence can be compensated if we readjust the LECs at different cutoffs.

There also exist other sources of uncertainties. First, we discuss the uncertainty from the resonance saturation model which is utilized to determine the LECs of the contact terms. From the numerical values of D_a and E_a in Eq. (29), we can see that the contributions from f_0 and a_0 are small, and the ρ, ω, and σ exchanges dominate D_a and E_a. For D_b and E_b in Eq. (29), the uncertainties from the axial-vector exchanges are not small, and therefore they have considerable effects on the binding energy. However, the estimation of the axial-vector contributions is quite rough, and we hope to obtain much more reliable input for g_{HHV_A} in the future. In general, the uncertainty in Eq. (29) gives a binding energy of $17.5^{+4.1+18.3}_{-3.9-14.0}$ MeV with, where the first uncertainty comes from f_0 and a_0, and the second uncertainty comes from axial-vector mesons (a_1, f_1).

Second, uncertainty can come from the axial coupling g. When we include the experimental error [101] (width and branching fraction), we obtain a bare coupling $g = 0.65^{+0.02}_{-0.01}$, and the binding energy in the $I = 0$ channel with $\Lambda = 0.7$ GeV is $17.5^{+9.6}_{-3.9}$ MeV. We can see that the binding energy is sensitive to the coupling g, but not much sensitive as cutoff Λ. Including the uncertainties from $D_{a(b)}$ and $E_{a(b)}$ discussed above, we obtain a binding energy of $17.5^{+21.1}_{-15.0}$ at $\Lambda = 0.7$ GeV. This uncertainty is largely due to axial-vector mesons, as the uncertainty from g is

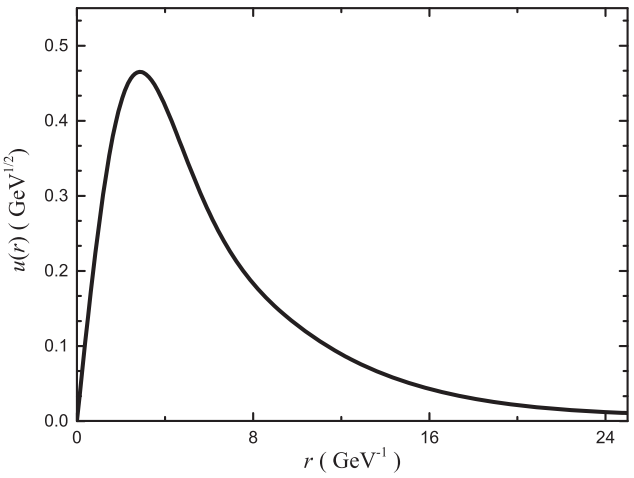

FIG. 10. The radial wave function with the full potential depicted in Fig. 8.

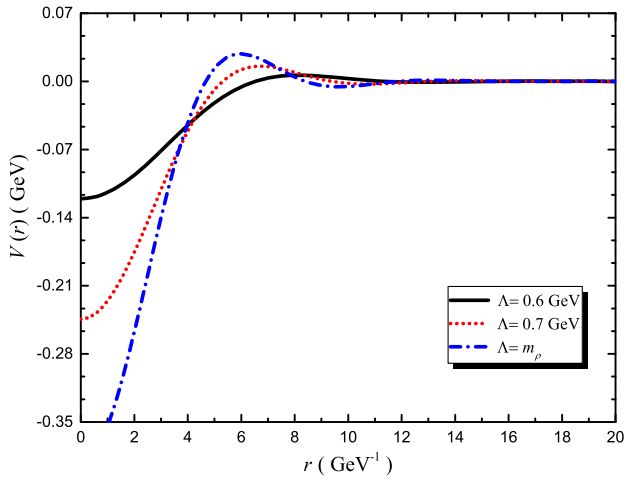

FIG. 11. The total potentials of the DD^* system in the S wave with $I = 0$, where three cutoff values are adopted.

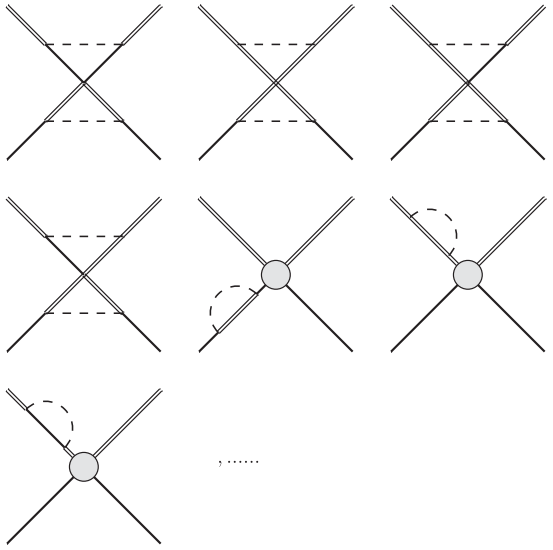

FIG. 12. Some loop diagrams related to contact terms at $O(\epsilon^4)$. The last three diagrams indicate the contribution from wave-function renormalization to the contact loop diagrams at $O(\epsilon^2)$ in Fig. 3.

moderate and the uncertainties from f_0 and a_0 are the smallest.

The third uncertainty comes from the truncation error. Here we partially estimate a few loop diagrams of the contact contribution at $O(\epsilon^4)$ to show how large the truncation error is. For the $O(\epsilon^4)$ contact loop contribution there are many Feynman diagrams. We pick some diagrams and plot them in Fig. 12. The first four diagrams of Fig. 12 each contain two separated loops, and the sum of these reads

$$\begin{aligned}\mathcal{V}^{(4)}_{I=1} &\sim (-0.00016-0.00015i)(D_a-D_b+E_a-E_b),\\ \mathcal{V}^{(4)}_{I=0} &\sim (-0.0039-0.0014i)D_a+(0.0117+0.0041i)E_a\\ &\quad+(0.0043+0.0019i)D_b-(0.0129+0.0057i)E_b.\end{aligned} \tag{31}$$

We can see that they are generally $O(\frac{1}{100})$ relative to those at $O(\epsilon^2)$ by comparing with Eqs. (21) and (23). The last three diagrams in Fig. 12 indicate the wave-function renormalization of the $O(\epsilon^2)$ diagrams in Fig. 3, and the sum of these reads

$$\begin{aligned}\mathcal{V}^{(4)}_{I=1} &\sim (0.0196+0.0060i)D_b-0.0034E_a\\ &\quad+(0.0127+0.0047i)E_b,\end{aligned} \tag{32}$$

$$\begin{aligned}\mathcal{V}^{(4)}_{I=0} &\sim (0.0934+0.0321i)E_a-(0.0085+0.0054i)D_b\\ &\quad-(0.0039-0.0110i)E_b.\end{aligned} \tag{33}$$

They are $O(\frac{1}{10})$ relative to those at $O(\epsilon^2)$ from Eqs. (21) and (23). Therefore, we expect that when all of the contact $O(\epsilon^4)$ diagrams are included the convergence may not be bad.

VI. SUMMARY

In this work, we systematically studied the DD^* system with ChEFT. Due to the intrinsic difficulty of ChEFT, we could not obtain the physical observables directly from the Feynman diagrams. Instead, we calculated the potentials, i.e., the sum of all of the 2PI diagrams, and then iterated them into the Lippmann-Schwinger or Schrödinger equation to recover the 2PR contributions.

We investigated the DD^* effective potentials in ChEFT using Weinberg's scheme. With the effective potentials obtained in momentum space, we analyzed the contact, OPE, and TPE contributions in detail. The OPE and TPE contributions are free of many LECs, and thus they are more model independent than the contact interaction since the LECs were determined with the resonance saturation model in this work. The OPE contribution at $O(\epsilon^2)$ is smaller than that at $O(\epsilon^0)$. The potential from TPE at $O(\epsilon^2)$ is relatively large compared to that from OPE at $O(\epsilon^0)$ in the $I=1$ channel, while it shows a good convergence in the $I=0$ channel. The TPE interaction is important and non-negligible.

We have determined the LECs in contact contributions with the resonance saturation model, and further explored the full potentials in coordinate space, which were regularized with a simple Gaussian cutoff. The roles of each contribution were discussed, and the total potentials are very different in the two channels. We also discussed the importance of the contact contribution and the influence of the cutoff in detail. Furthermore, we discussed the uncertainties of our approach, which come from the axial coupling g, the LECs, and the truncation error. We found that the TPE contribution is non-negligible and attractive in general, while the contact contributions are an important element and compete with the π-exchange contributions to cause quite different behavior in each of the channels. Despite the roughly estimated LECs, we found that there is no bound state in the $I=1$ channel for a wide range of the cutoff parameter, while there is a bound state in the $I=1$ channel as the cutoff is near m_ρ in our approach. The binding energy is sensitive to the cutoff. Our results are consistent with those in the one-boson-exchange model [76].

In this work we ignored many other subleading effects, such as isospin violation, S-D mixing, recoil, and so on. These effects can be investigated in the future, and our framework shall be proved to be elegant.

We point out that the DD^* molecule may be discovered at experiments through various processes. Since at the Tevatron and LHCb there are a number of B_c events, the DD^* molecule can be produced via B_c weak decays: the singly Cabibbo-suppressed process $B_c \to X(DD^*)K$, and

the doubly Cabibbo-suppressed processes $B_c \to X(DD^*)\pi$ and $B_c \to X(DD^*)D$. Moreover, we hope the e^+e^- processes such as $e^+e^- \to X(DD^*)\bar{D}\,\bar{D}$ at Belle II can be studied to observe this state. The molecular states may be constructed through DD final states. We also expect that lattice simulations could be used to test our results.

Our exploration of the DD^* system can help to provide a more profound understanding of the heavy meson system and nonperturbative QCD. We expect that our results could be tested by future LHCb and Belle II experiments and help the extrapolations of future lattice simulations.

ACKNOWLEDGMENTS

We would like to thank Professor Shi-Lin Zhu for useful suggestions. H. X. also thanks Rui Chen and Ming-Xiao Duan for helpful discussions. This project is supported by the National Natural Science Foundation of China under Grant No. 11705072. This work is also supported by the Fundamental Research Funds for the Central Universities. X. L. is also supported by the China National Funds for Distinguished Young Scientists under Grant No. 11825503.

APPENDIX A: ONE-LOOP AMPLITUDES OF THE PROCESSES $DD^* \to DD^*$ AT $O(\epsilon^2)$

We first list the amplitudes of the process $D(p_1)D^*(p_2) \to D(p_3)D^*(p_4)$. The difference between the amplitudes for the $I = 0$ and $I = 1$ channels is just a factor.

For the one-loop corrections to the contact terms in Fig. 3, the Feynman amplitudes are

$$\mathcal{M}^{(2)}_{(a1)} = \frac{-i}{4}\frac{g^2}{f^2}A_{a1}J^q_{22}(m,\omega_1,\omega_2)\varepsilon(p_2)\cdot\varepsilon^*(p_4)$$
$$\text{with}\quad \omega_1 = v\cdot p_2 - M, \qquad \omega_2 = v\cdot p_4 - M; \tag{A1}$$

$$\mathcal{M}^{(2)}_{(a2)} = \frac{-i}{2}\frac{g^2}{f^2}A_{a2}J^q_{22}(m,\omega_1,\omega_2)\varepsilon(p_2)\cdot\varepsilon^*(p_4)$$
$$\text{with}\quad \omega_1 = v\cdot p_2 - M - \delta, \qquad \omega_2 = v\cdot p_4 - M - \delta; \tag{A2}$$

$$\mathcal{M}^{(2)}_{(a3)} = \frac{i}{4}\frac{g^2}{f^2}A_{a3}J^g_{22}(m,\omega_1,\omega_2)\varepsilon(p_2)\cdot\varepsilon^*(p_4)$$
$$\text{with}\quad \omega_1 = v\cdot p_2 - M, \qquad \omega_2 = v\cdot p_3 - M - \delta; \tag{A3}$$

$$\mathcal{M}^{(2)}_{(a4)} = \frac{-i}{4}\frac{g^2}{f^2}A_{a4}J^g_{22}(m,\omega_1,\omega_2)\varepsilon(p_2)\cdot\varepsilon^*(p_4)$$
$$\text{with}\quad \omega_1 = v\cdot p_1 - M - \delta, \qquad \omega_2 = v\cdot p_3 - M - \delta; \tag{A4}$$

$$\mathcal{M}^{(2)}_{(a5)} = \frac{i}{4}\frac{g^2}{f^2}A_{a5}J^g_{22}(m,\omega_1,\omega_2)\varepsilon(p_2)\cdot\varepsilon^*(p_4)$$
$$\text{with}\quad \omega_1 = v\cdot p_1 - M - \delta, \qquad \omega_2 = v\cdot p_4 - M; \tag{A5}$$

$$\mathcal{M}^{(2)}_{(a6)} = \frac{i}{4}\frac{g^2}{f^2}A_{a6}J^h_{22}(m,\omega_2,\omega_1)\varepsilon(p_2)\cdot\varepsilon^*(p_4)$$
$$\text{with}\quad \omega_1 = v\cdot p_1 - M - \delta, \qquad \omega_2 = v\cdot p_2 - M; \tag{A6}$$

$$\mathcal{M}^{(2)}_{(a7)} = \frac{i}{4}\frac{g^2}{f^2}A_{a7}J^h_{22}(m,\omega_2,\omega_1)\varepsilon(p_2)\cdot\varepsilon^*(p_4)$$
$$\text{with}\quad \omega_1 = v\cdot p_4 - M, \qquad \omega_2 = v\cdot p_3 - M - \delta; \tag{A7}$$

$$\mathcal{M}^{(2)}_{(a8)} = \frac{-i}{2}\frac{g^2}{f^2}A_{a8}J^h_{22}(m,\omega_2,\omega_1)\varepsilon(p_2)\cdot\varepsilon^*(p_4)$$
$$\text{with}\quad \omega_1 = v\cdot p_1 - M - \delta, \qquad \omega_2 = v\cdot p_2 - M - \delta; \tag{A8}$$

$$\mathcal{M}^{(2)}_{(a9)} = \frac{-i}{2}\frac{g^2}{f^2}A_{a9}J^h_{22}(m,\omega_2,\omega_1)\varepsilon(p_2)\cdot\varepsilon^*(p_4)$$
$$\text{with}\quad \omega_1 = v\cdot p_4 - M - \delta, \qquad \omega_2 = v\cdot p_3 - M - \delta; \tag{A9}$$

$$\mathcal{M}^{(2)}_{(a10)} = \frac{i}{2}\frac{g^2}{f^2}A_{a10}J^g_{22}(m,\omega_1,\omega_2)\varepsilon(p_2)\cdot\varepsilon^*(p_4)$$
$$\text{with}\quad \omega_1 = v\cdot p_2 - M - \delta, \qquad \omega_2 = v\cdot p_3 - M - \delta; \tag{A10}$$

$$\mathcal{M}^{(2)}_{(a11)} = \frac{i}{2}\frac{g^2}{f^2}A_{a11}J^g_{22}(m,\omega_1,\omega_2)\varepsilon(p_2)\cdot\varepsilon^*(p_4)$$
$$\text{with}\quad \omega_1 = v\cdot p_1 - M - \delta, \qquad \omega_2 = v\cdot p_4 - M - \delta; \tag{A11}$$

$$\mathcal{M}^{(2)}_{(a12+a13)} = -i\frac{g^2}{f^2}A_{a12a13} \times\left(\frac{3}{8}\partial\omega J^b_{22}(m,\omega_1) + \frac{3}{4}\partial\omega J^b_{22}(m,\omega_2)\right) \times\varepsilon(p_2)\cdot\varepsilon^*(p_4)$$
$$\text{with}\ \omega_1 = v\cdot p_2 - M,\ \omega_2 = v\cdot p_2 - M - \delta,\ \text{and with}\ \omega_1 = v\cdot p_4 - M, \omega_2 = v\cdot p_4 - M - \delta; \tag{A12}$$

$$\mathcal{M}^{(2)}_{(a14)} = -i\frac{g^2}{f^2}A_{a14}\left(\frac{9}{8}\partial\omega J^b_{22}(m,\omega_1)\right)\varepsilon(p_2)\cdot\varepsilon^*(p_4)$$
$$\text{with}\quad \omega_1 = v\cdot p_1 - M - \delta,\quad \text{and with}\quad \omega_1 = v\cdot p_3 - M - \delta. \tag{A13}$$

For the one-loop corrections to the OPE potentials in Fig. 4, the Feynman amplitudes are

$$\mathcal{M}^{(2)}_{(b1)} = \frac{i}{4}\frac{g^4}{f^4}A_{b1}\frac{p_\mu p_\nu}{p^2 - m^2}J^g_{22}(m,\omega_1,\omega_2)\varepsilon^\mu(p_2)\varepsilon^{*\nu}(p_4)$$
$$\text{with}\quad \omega_1 = v\cdot p_3 - M - \delta, \qquad \omega_2 = v\cdot p_2 - M; \tag{A14}$$

$$\mathcal{M}^{(2)}_{(b2)} = \frac{i}{2}\frac{g^4}{f^4}A_{b2}\frac{p_\mu p_\nu}{p^2-m^2}J^g_{22}(m,\omega_1,\omega_2)\varepsilon^\mu(p_2)\varepsilon^{*\nu}(p_4)$$
$$\text{with}\quad \omega_1 = v\cdot p_2 - M - \delta, \qquad \omega_2 = v\cdot p_3 - M - \delta; \tag{A15}$$

$$\mathcal{M}^{(2)}_{(b3)} = \frac{i}{4}\frac{g^4}{f^4}A_{b3}\frac{p_\mu p_\nu}{p^2-m^2}J^g_{22}(m,\omega_1,\omega_2)\varepsilon^\mu(p_2)\varepsilon^{*\nu}(p_4)$$
$$\text{with}\quad \omega_1 = v\cdot p_1 - M - \delta, \quad \omega_2 = v\cdot p_4 - M; \tag{A16}$$

$$\mathcal{M}^{(2)}_{(b4)} = \frac{i}{2}\frac{g^4}{f^4}A_{b4}\frac{p_\mu p_\nu}{p^2-m^2}J^g_{22}(m,\omega_1,\omega_2)\varepsilon^\mu(p_2)\varepsilon^{*\nu}(p_4)$$
$$\text{with}\quad \omega_1 = v\cdot p_1 - M - \delta, \qquad \omega_2 = v\cdot p_4 - M - \delta; \tag{A17}$$

$$\mathcal{M}^{(2)}_{(b5)} = i\frac{g^2}{f^4}A_{b5}\frac{p_\mu p_\nu}{p^2-m^2}\left[2m^2L + \frac{2m^2}{16\pi^2}\log\left(\frac{m}{\mu}\right)\right] \times \varepsilon^\mu(p_2)\varepsilon^{*\nu}(p_4); \tag{A18}$$

$$\mathcal{M}^{(2)}_{(b6)} = i\frac{g^2}{f^4}A_{b6}\frac{p_\mu p_\nu}{p^2-m^2}\left[2m^2L + \frac{2m^2}{16\pi^2}\log\left(\frac{m}{\mu}\right)\right] \times \varepsilon^\mu(p_2)\varepsilon^{*\nu}(p_4); \tag{A19}$$

$$\mathcal{M}^{(2)}_{(b7)} = i\frac{g^2}{f^2}A_{b7}\frac{p_\mu p_\nu}{p^2-m^2}\left[\frac{2}{3f^2}\left(2m^2L + \frac{2m^2}{16\pi^2}\log\left(\frac{m}{\mu}\right)\right)\right] \times \varepsilon^\mu(p_2)\varepsilon^{*\nu}(p_4); \tag{A20}$$

$$\mathcal{M}^{(2)}_{(b8)} = 0; \qquad \mathcal{M}^{(2)}_{(b9)} = 0; \tag{A21}$$

$$\mathcal{M}^{(2)}_{(b10+b11)} = -i\frac{g^4}{f^4}A_{b10b11}\frac{p_\mu p_\nu}{p^2-m^2} \times \left(\frac{3}{8}\partial\omega J^b_{22}(m,\omega_1) + \frac{3}{4}\partial\omega J^b_{22}(m,\omega_2)\right) \times \varepsilon^\mu(p_2)\varepsilon^{*\nu}(p_4)$$
$$\text{with } \omega_1 = v\cdot p_2 - M,\ \omega_2 = v\cdot p_2 - M - \delta, \text{ and with } \omega_1 = v\cdot p_4 - M, \quad \omega_2 = v\cdot p_4 - M - \delta; \tag{A22}$$

$$\mathcal{M}^{(2)}_{(b12)} = -i\frac{g^4}{f^4}A_{b12}\frac{p_\mu p_\nu}{p^2-m^2}\left(\frac{9}{8}\partial\omega J^b_{22}(m,\omega_1)\right) \times \varepsilon^\mu(p_2)\varepsilon^{*\nu}(p_4)$$
$$\text{with}\quad \omega_1 = v\cdot p_1 - M - \delta, \quad \text{and} \quad \text{with} \quad \omega_1 = v\cdot p_3 - M - \delta. \tag{A23}$$

For the TPE potentials in Fig. 5, the Feynman amplitudes are

$$\mathcal{M}^{(2)}_{(c1)} = \frac{i}{4f^4}[4A_{c1a}(q_0^2J^F_{21} + J^F_{22}) + 4A_{c1b}q_0^2J^F_{11} + A_{c1c}J^F_0] \times \varepsilon(p_2)\cdot\varepsilon^*(p_4); \tag{A24}$$

$$\mathcal{M}^{(2)}_{(c2)} = \frac{-i}{4}\frac{g^2}{f^4}A_{c2}[(2A_{c2c}q_0J^S_{31} + 2A_{c2c}J^S_{34} + A_{c2d}q_0J^S_{21}) \times \varepsilon(p_2)\cdot\varepsilon^*(p_4) + (2A_{c2c}q_0J^S_{32} + 2A_{c2c}J^S_{33} + (A_{c2d}+2A_{c2c})q_0J^S_{22} + 2A_{c2c}J^S_{24} + A_{c2d}q_0J^S_{11}) \times q\cdot\varepsilon(p_2)q\cdot\varepsilon^*(p_4)]$$
$$\text{with}\quad \omega = v\cdot p_2 - M; \tag{A25}$$

$$\mathcal{M}^{(2)}_{(c3)} = \frac{i}{4}\frac{g^2}{f^4}A_{c3}[(2A_{c3d}q_0J^S_{21} - (2A_{c3c}+A_{c3d})q_0\vec{q}^2J^S_{22} - 2A_{c3c}\vec{q}^2J^S_{24} + 4A_{c3c}q_0J^S_{31} - 2A_{c3c}q_0\vec{q}^2J^S_{32} - 2A_{c3c}\vec{q}^2J^S_{33} + 4A_{c3c}J_{34} - A_{c3d}q_0\vec{q}^2J^S_{11})\varepsilon(p_2) \cdot\varepsilon^*(p_4) + (-A_{c3d}q_0J^S_{11} - (2A_{c3c}+A_{c3d})q_0J^S_{22} - 2A_{c3c}J^S_{24} - 2A_{c3c}q_0J^S_{32} - 2A_{c3c}J^S_{33})q\cdot\varepsilon(p_2)q\cdot\varepsilon^*(p_4)]$$
$$\text{with}\quad \omega = v\cdot p_2 - M - \delta; \tag{A26}$$

$$\mathcal{M}^{(2)}_{(c4)} = \frac{i}{4}\frac{g^2}{f^4}[A_{c4d}q_0\vec{q}^2J^T_{11} - 3A_{c4d}q_0J^T_{21} + (2A_{c4c}+A_{c4d})q_0\vec{q}^2J^T_{22} + 2A_{c4c}\vec{q}^2J^T_{24} - 6A_{c4c}q_0J^T_{31} + 2A_{c4c}q_0\vec{q}^2J^T_{32} + 2A_{c4c}\vec{q}^2J^T_{33} - 6A_{c4c}J^T_{34}]\varepsilon(p_2)\cdot\varepsilon^*(p_4)$$
$$\text{with}\quad \omega = v\cdot p_1 - M - \delta; \tag{A27}$$

$$\mathcal{M}^{(2)}_{(c5)} = \frac{i}{4}\frac{g^4}{f^4}A_{c5}[(-\vec{q}^2J^B_{31} + 5J^B_{41} - \vec{q}^2J^B_{42})\varepsilon(p_2) \cdot\varepsilon^*(p_4) + (J^B_{21} - \vec{q}^2J^B_{22} + 7J^B_{31} - 2\vec{q}^2J^B_{32} + 7J^B_{42} - \vec{q}^2J^B_{43}) \times q\cdot\varepsilon(p_2)q\cdot\varepsilon^*(p_4)]$$
$$\text{with}\quad \omega_1 = v\cdot p_1 - M - \delta, \quad \omega_2 = v\cdot p_2 - M; \tag{A28}$$

$$\mathcal{M}^{(2)}_{(c6)} = \frac{-i}{4}\frac{g^4}{f^4}A_{c6}[(-\vec{q}^2J^B_{21} + (\vec{q}^2)^2J^B_{22} - 9\vec{q}^2J^B_{31} + 2(\vec{q}^2)^2J^B_{32} + 10J^B_{41} - 9\vec{q}^2J^B_{42} + (\vec{q}^2)^2J^B_{43})\varepsilon(p_2)\cdot\varepsilon^*(p_4) + (-J^B_{21} + \vec{q}^2J^B_{22} - 7J^B_{31} + 2\vec{q}^2J^B_{32} - 7J^B_{42} + \vec{q}^2J^B_{43}) \times q\cdot\varepsilon(p_2)q\cdot\varepsilon^*(p_4)]$$
$$\text{with}\quad \omega_1 = v\cdot p_1 - M - \delta, \qquad \omega_2 = v\cdot p_2 - M - \delta; \tag{A29}$$

TABLE I. The coefficients for the contact amplitudes in the processes $DD^* \to DD^*$.

	$I=1$	$I=0$
A_{a1}	$-32D_a-32E_a$	$-48D_a-48E_a$
A_{a2}	$8D_b-24D_a+8E_a+40E_b$	$24D_b-24D_a-24E_a+24E_b$
A_{a3}	$-32D_b-32E_b$	$48D_b+48E_b$
A_{a4}	$16D_b-80D_a-16E_a+80E_b$	$48D_b-96D_a-96E_a+48E_b$
A_{a5}	$-32D_b-32E_b$	$48D_b+48E_b$
A_{a6}	$8D_a-8D_b+8E_a-8E_b$	$24D_a+24D_b-72E_a-72E_b$
A_{a7}	$8D_a-8D_b+8E_a-8E_b$	$24D_a+24D_b-72E_a-72E_b$
A_{a8}	0	$-48D_b+144E_b$
A_{a9}	0	$-48D_b+144E_b$
A_{a10}	$16D_b-48E_b$	0
A_{a11}	$16D_b-48E_b$	0
A_{a12a13}	$-8D_a+8D_b-8E_a+8E_b$	$-8D_a-8D_b+24E_a+24E_b$
A_{a14}	$-8D_a+8D_b-8E_a+8E_b$	$-8D_a-8D_b+24E_a+24E_b$

$$\mathcal{M}^{(2)}_{(c7)}=\frac{-i}{4}\frac{g^4}{f^4}A_{c7}[\vec{p}^2J^B_{21}\varepsilon(p_2)\cdot\varepsilon^*(p_4)+J^B_{21}p\cdot\varepsilon(p_2)p\cdot\varepsilon^*(p_4)]$$
$$\text{with}\quad \omega_1=v\cdot p_1-M-\delta,\qquad \omega_2=v\cdot p_2-M-\delta; \tag{A30}$$

$$\mathcal{M}^{(2)}_{(c8)}=\frac{i}{4}\frac{g^4}{f^4}A_{c8}[(-\vec{q}^2J^R_{31}+5J^R_{41}-\vec{q}^2J^R_{42})\varepsilon(p_2)\cdot\varepsilon^*(p_4)+(J^R_{21}-\vec{q}^2J^R_{22}+7J^R_{31}-2\vec{q}^2J^R_{32}+7J^R_{42}-\vec{q}^2J^R_{43})\times q\cdot\varepsilon(p_2)q\cdot\varepsilon^*(p_4)]$$
$$\text{with}\quad \omega_1=v\cdot p_1-M-\delta,\qquad \omega_2=v\cdot p_2; \tag{A31}$$

$$\mathcal{M}^{(2)}_{(c9)}=\frac{-i}{4}\frac{g^4}{f^4}A_{c9}[(-\vec{q}^2J^R_{21}+(\vec{q}^2)^2J^R_{22}-9\vec{q}^2J^R_{31}+2(\vec{q}^2)^2J^R_{32}+10J^R_{41}-9\vec{q}^2J^R_{42}+(\vec{q}^2)^2J^R_{43})\varepsilon(p_2)\cdot\varepsilon^*(p_4)+(-J^R_{21}+\vec{q}^2J^R_{22}-7J^R_{31}+2\vec{q}^2J^R_{32}-7J^R_{42}+\vec{q}^2J^R_{43})\times q\cdot\varepsilon(p_2)q\cdot\varepsilon^*(p_4)]$$
$$\text{with}\quad \omega_1=v\cdot p_1-M-\delta,\qquad \omega_2=v\cdot p_2-M-\delta. \tag{A32}$$

$$\mathcal{M}^{(2)}_{(c10)}=\frac{i}{4}\frac{g^4}{f^4}A_{c10}[\vec{p}^2J^R_{21}\varepsilon(p_2)\cdot\varepsilon^*(p_4)+J^R_{21}p\cdot\varepsilon(p_2)p\cdot\varepsilon^*(p_4)]$$
$$\text{with}\quad \omega_1=v\cdot p_1-M-\delta,\qquad \omega_2=v\cdot p_2-M-\delta. \tag{A33}$$

In the above expressions, J^F_{ij} is shorthand notation for $J^F_{ij}(m_1,m_2,q)$, and J^S_{ij} and J^T_{ij} are $J^S_{ij}(m_1,m_2,\omega,q)$ and $J^T_{ij}(m_1,m_2,\omega,q)$, respectively. J^B_{ij} and J^R_{ij} are $J^B_{ij}(m_1,m_2,\omega_1,\omega_2,q)$ and $J^R_{ij}(m_1,m_2,\omega_1,\omega_2,q)$, respectively. These loop functions (like J^q) are defined in Appendix C.

In Eqs. (A1)–(A33), the constants A are different for different isospins. We list them in Tables I–III. The remaining constants are

$$A_{c1b}=1,\quad A_{c1c}=q_0^2,\quad A_{c2c}=-1,\quad A_{c2d}=-1,\quad A_{c3c}=-1,\quad A_{c3d}=-1,\quad A_{c4c}=1,\quad A_{c4d}=1 \tag{A34}$$

for $I=1$, and

$$A_{c1b}=-3,\quad A_{c1c}=-3q_0^2,\quad A_{c2c}=3,\quad A_{c2d}=3,\quad A_{c3c}=3,\quad A_{c3d}=3,\quad A_{c4c}=-3,\quad A_{c4d}=-3 \tag{A35}$$

for $I=0$.

TABLE II. The coefficients for the OPE amplitudes in the processes $DD^* \to DD^*$.

	A_{b1}	A_{b2}	A_{b3}	A_{b4}	A_{b5}	A_{b6}	A_{b7}	A_f	A_{b10b11}	A_{b12}
$I=1$	−1	1	−1	1	1/3	1/3	−1	−1	−1	−1
$I=0$	−3	3	−3	3	1	1	−3	−3	−3	−3

TABLE III. The coefficients for the TPE amplitudes in the processes $DD^* \to DD^*$.

	A_{c1a}	A_{c2}	A_{c3}	A_{c4}	A_{c5}	A_{c6}	A_{c7}	A_{c8}	A_{c9}	A_{c10}
$I=1$	1	−2	2	−2	1	−1	−1	5	−5	−5
$I=0$	−3	−2	2	−2	9	−9	9	−3	3	−3

In Eqs. (A1)–(A33), M is the D meson mass, δ is the mass difference between D^* and D, m, m_1, and m_2 are all pion masses, $p = p_1 - p_4$, $q = p_1 - p_3$, μ is the renormalization scale in the dimensional regularization, and

$$L = \frac{1}{16\pi^2}\left(\frac{1}{d-4} + \frac{1}{2}(\gamma_E - 1 - \log 4\pi)\right). \tag{A36}$$

APPENDIX B: RENORMALIZED AND BARE COUPLINGS

The relation between the experimental renormalized coupling $g^{(2)}$ and the bare coupling g in the Lagrangian is

$$g^{(2)} = g\left(1 - \frac{g^2}{2f^2}J^g_{22}(0,-\delta) + \frac{g^2}{4f^2}J^g_{22}(-\delta,\delta) - \frac{9g^2}{8f^2}\partial J^b_{22}(-\delta) - \frac{3g^2}{8f^2}\partial J^b_{22}(\delta) - \frac{3g^2}{4f^2}\partial J^b_{22}(0)\right). \tag{B1}$$

The expression relating the renormalized $f_{(2)}$ and the bare f is well known:

$$\frac{1}{f^2_{(2)}} = \frac{1}{f^2}\left(1 + \frac{m^2}{4\pi f^2}\log\left(\frac{m}{\mu}\right)\right). \tag{B2}$$

We use $f_{(2)} = f_\pi = 0.092$ GeV.

APPENDIX C: DEFINITIONS OF SOME LOOP FUNCTIONS

We define the loop functions following Ref. [82]:

$$i\int\frac{d^Dl\mu^{4-D}}{(2\pi)^D}\frac{\{1, l^\alpha, l^\alpha l^\beta, l^\alpha l^\beta l^\gamma\}}{[(+/-)v\cdot l + \omega + i\varepsilon](l^2 - m^2 + i\varepsilon)} \equiv \{J^{a/b}_0, v^\alpha J^{a/b}_{11}, v^\alpha v^\beta J^{a/b}_{21} + g^{\alpha\beta}J^{a/b}_{22}, (g\vee v)J^{a/b}_{31} + v^\alpha v^\beta v^\gamma J^{a/b}_{32}\}(m,\omega), \tag{C1}$$

$$\begin{aligned} &i\int\frac{d^Dl\mu^{4-D}}{(2\pi)^D}\frac{\{1, l^\alpha, l^\alpha l^\beta, l^\alpha l^\beta l^\gamma\}}{(v\cdot l + \omega_1 + i\varepsilon)[(+/-)v\cdot l + \omega_2 + i\varepsilon](l^2 - m^2 + i\varepsilon)} \\ &\equiv \{J^{g/h}_0, v^\alpha J^{g/h}_{11}, v^\alpha v^\beta J^{g/h}_{21} + g^{\alpha\beta}J^{g/h}_{22}, (g\vee v)J^{g/h}_{31} + v^\alpha v^\beta v^\gamma J^{g/h}_{32}\}(m,\omega_1,\omega_2), \end{aligned} \tag{C2}$$

$$i\int\frac{d^Dl\mu^{4-D}}{(2\pi)^D}\frac{\{1, l^\alpha, l^\alpha l^\beta, l^\alpha l^\beta l^\gamma\}}{(l^2 - m_1^2 + i\varepsilon)[(q+l)^2 - m_2^2 + i\varepsilon]} \equiv \{J^F_0, q^\alpha J^F_{11}, q^\alpha q^\beta J^F_{21} + g^{\alpha\beta}J^F_{22}, (g\vee q)J^F_{31} + q^\alpha q^\beta q^\gamma J^F_{32}\}(m_1,m_2,q), \tag{C3}$$

$$\begin{aligned} &i\int\frac{d^Dl\mu^{4-D}}{(2\pi)^D}\frac{\{1, l^\alpha, l^\alpha l^\beta, l^\alpha l^\beta l^\gamma, l^\alpha l^\beta l^\gamma l^\delta\}}{[(+/-)v\cdot l + \omega + i\varepsilon](l^2 - m_1^2 + i\varepsilon)[(q+l)^2 - m_2^2 + i\varepsilon]} \\ &\equiv \{J^{T/S}_0, q^\alpha J^{T/S}_{11} + v^\alpha J^{T/S}_{12}, g^{\alpha\beta}J^{T/S}_{21} + q^\alpha q^\beta J^{T/S}_{22} + v^\alpha v^\beta J^{T/S}_{23} + (q\vee v)J^{T/S}_{24}, (g\vee q)J^{T/S}_{31} + q^\alpha q^\beta q^\gamma J^{T/S}_{32} + (q^2\vee v)J^{T/S}_{33} \\ &+ (g\vee v)J^{T/S}_{34} + (q\vee v^2)J^{T/S}_{35} + v^\alpha v^\beta v^\gamma J^T_{36}, (g\vee g)J^{T/S}_{41} + (g\vee q^2)J^{T/S}_{42} + q^\alpha q^\beta q^\gamma q^\delta J^{T/S}_{43} + (g\vee v^2)J^{T/S}_{44} + v^\alpha v^\beta v^\gamma v^\delta J^{T/S}_{45} \\ &+ (q^3\vee v)J^{T/S}_{46} + (q^2\vee v^2)J^{T/S}_{47} + (q\vee v^3)J^{T/S}_{48} + (g\vee q\vee v)J^{T/S}_{49}\}(m_1,m_2,\omega,q), \end{aligned} \tag{C4}$$

$$\begin{aligned} &i\int\frac{d^Dl\mu^{4-D}}{(2\pi)^D}\frac{\{1, l^\alpha, l^\alpha l^\beta, l^\alpha l^\beta l^\gamma, l^\alpha l^\beta l^\gamma l^\delta\}}{(v\cdot l + \omega_1 + i\varepsilon)[(+/-)v\cdot l + \omega_2 + i\varepsilon](l^2 - m_1^2 + i\varepsilon)[(q+l)^2 - m_2^2 + i\varepsilon]} \\ &\equiv \{J^{R/B}_0, q^\alpha J^{R/B}_{11} + v^\alpha J^{R/B}_{12}, g^{\alpha\beta}J^{R/B}_{21} + q^\alpha q^\beta J^{R/B}_{22} + v^\alpha v^\beta J^{R/B}_{23} + (q\vee v)J^{R/B}_{24}, (g\vee q)J^{R/B}_{31} + q^\alpha q^\beta q^\gamma J^{R/B}_{32} + (q^2\vee v)J^{R/B}_{33} \\ &+ (g\vee v)J^{R/B}_{34} + (q\vee v^2)J^{R/B}_{35} + v^\alpha v^\beta v^\gamma J^{R/B}_{36}, (g\vee g)J^{R/B}_{41} + (g\vee q^2)J^{R/B}_{42} + q^\alpha q^\beta q^\gamma q^\delta J^{R/B}_{43} + (g\vee v^2)J^{R/B}_{44} + v^\alpha v^\beta v^\gamma v^\delta J^{R/B}_{45} \\ &+ (q^3\vee v)J^{R/B}_{46} + (q^2\vee v^2)J^{R/B}_{47} + (q\vee v^3)J^{R/B}_{48} + (g\vee q\vee v)J^{R/B}_{49}\}(m_1,m_2,\omega_1,\omega_2,q), \end{aligned} \tag{C5}$$

with

$$
\begin{aligned}
&q \vee v \equiv q^\alpha v^\beta + q^\beta v^\alpha, \qquad g \vee q \equiv g^{\alpha\beta} q^\gamma + g^{\alpha\gamma} q^\beta + g^{\gamma\beta} q^\alpha, \qquad g \vee v \equiv g^{\alpha\beta} v^\gamma + g^{\alpha\gamma} v^\beta + g^{\gamma\beta} v^\alpha,\\
&q^2 \vee v \equiv q^\beta q^\gamma v^\alpha + q^\alpha q^\gamma v^\beta + q^\alpha q^\beta v^\gamma, \qquad q \vee v^2 \equiv q^\gamma v^\alpha v^\beta + q^\beta v^\alpha v^\gamma + q^\alpha v^\beta v^\gamma,\\
&g \vee g \equiv g^{\alpha\beta} g^{\gamma\delta} + g^{\alpha\delta} g^{\beta\gamma} + g^{\alpha\gamma} g^{\beta\delta}, \qquad g \vee q^2 \equiv q^\alpha q^\beta g^{\gamma\delta} + q^\alpha q^\delta g^{\beta\gamma} + q^\alpha q^\gamma g^{\beta\delta} + q^\gamma q^\delta g^{\alpha\beta} + q^\beta q^\delta g^{\alpha\gamma} + q^\beta q^\gamma g^{\alpha\delta},\\
&g \vee v^2 \equiv v^\alpha v^\beta g^{\gamma\delta} + v^\alpha v^\delta g^{\beta\gamma} + v^\alpha v^\gamma g^{\beta\delta} + v^\gamma v^\delta g^{\alpha\beta} + v^\beta v^\delta g^{\alpha\gamma} + v^\beta v^\gamma g^{\alpha\delta},\\
&q^3 \vee v \equiv q^\beta q^\gamma q^\delta v^\alpha + q^\alpha q^\gamma q^\delta v^\beta + q^\alpha q^\beta q^\delta v^\gamma + q^\alpha q^\beta q^\gamma v^\delta, \qquad q \vee v^3 \equiv q^\delta v^\alpha v^\beta v^\gamma + q^\gamma v^\alpha v^\beta v^\delta + q^\beta v^\alpha v^\gamma v^\delta + q^\alpha v^\beta v^\gamma v^\delta,\\
&q^2 \vee v^2 \equiv q^\gamma q^\delta v^\alpha v^\beta + q^\beta q^\delta v^\alpha v^\gamma + q^\alpha q^\delta v^\beta v^\gamma + q^\beta q^\gamma v^\alpha v^\delta + q^\alpha q^\gamma v^\beta v^\delta + q^\alpha q^\beta v^\gamma v^\delta,\\
&g \vee q \vee v \equiv q^\beta v^\alpha g^{\gamma\delta} + q^\alpha v^\beta g^{\gamma\delta} + q^\delta v^\alpha g^{\beta\gamma} + q^\gamma v^\alpha g^{\beta\delta} + q^\alpha v^\delta g^{\beta\gamma} + q^\alpha v^\gamma g^{\beta\delta} + q^\delta v^\gamma g^{\alpha\beta} + q^\delta v^\beta g^{\alpha\gamma} + q^\gamma v^\delta g^{\alpha\beta}\\
&\qquad + q^\gamma v^\beta g^{\alpha\delta} + q^\beta v^\delta g^{\alpha\gamma} + q^\beta v^\gamma g^{\alpha\delta}.
\end{aligned} \tag{C6}
$$

J^b is related to J^a as

$$
\begin{aligned}
&J^b_0 = J^a_0, \qquad J^b_{11} = -J^a_{11}, \qquad J^b_{21} = J^a_{21}, \qquad J^b_{22} = J^a_{22},\\
&J^b_{31} = -J^a_{31}, \qquad J^b_{32} = -J^a_{32}.
\end{aligned} \tag{C7}
$$

J^g and J^h can be reduced to

$$
J^g(\omega_1, \omega_2) = \frac{1}{\omega_2 - \omega_1}[J^a(\omega_1) - J^a(\omega_2)], \tag{C8}
$$

$$
J^h(\omega_1, \omega_2) = \frac{1}{\omega_2 + \omega_1}[J^a(\omega_1) + J^b(\omega_2)]. \tag{C9}
$$

J^S is related to J^T as

$$
\begin{aligned}
&J^S_0(v\cdot q) = J^T_0(-v\cdot q), \qquad J^S_{11}(v\cdot q) = J^T_{11}(-v\cdot q),\\
&J^S_{12}(v\cdot q) = -J^T_{12}(-v\cdot q), \qquad J^S_{21} = J^T_{21}(-v\cdot q),\\
&J^S_{22}(v\cdot q) = J^T_{22}(-v\cdot q), \qquad J^S_{23}(v\cdot q) = J^T_{23}(-v\cdot q).\\
&J^S_{24}(v\cdot q) = -J^T_{24}(-v\cdot q), \qquad J^S_{31}(v\cdot q) = J^T_{31}(-v\cdot q).\\
&J^S_{32}(v\cdot q) = J^T_{32}(-v\cdot q), \qquad J^S_{33}(v\cdot q) = -J^T_{33}(-v\cdot q).\\
&J^S_{34}(v\cdot q) = -J^T_{34}(-v\cdot q), \qquad J^S_{35}(v\cdot q) = J^T_{35}(-v\cdot q).\\
&J^S_{36}(v\cdot q) = -J^T_{34}(-v\cdot q), \qquad J^S_{41}(v\cdot q) = J^T_{41}(-v\cdot q).\\
&J^S_{42}(v\cdot q) = J^T_{42}(-v\cdot q), \qquad J^S_{43}(v\cdot q) = J^T_{43}(-v\cdot q).\\
&J^S_{44}(v\cdot q) = J^T_{44}(-v\cdot q), \qquad J^S_{45}(v\cdot q) = J^T_{45}(-v\cdot q).\\
&J^S_{46}(v\cdot q) = -J^T_{46}(-v\cdot q), \qquad J^S_{47}(v\cdot q) = J^T_{47}(-v\cdot q).\\
&J^S_{48}(v\cdot q) = -J^T_{48}(-v\cdot q), \qquad J^S_{49}(v\cdot q) = -J^T_{49}(-v\cdot q).
\end{aligned} \tag{C10}
$$

J^R and J^B can be reduced to

$$
J^R(\omega_1, \omega_2) = \frac{1}{\omega_2 - \omega_1}[J^T(\omega_1) - J^T(\omega_2)], \tag{C11}
$$

$$
J^B(\omega_1, \omega_2) = \frac{1}{\omega_2 + \omega_1}[J^T(\omega_1) + J^S(\omega_2)]. \tag{C12}
$$

All of the integrals in Eqs. (C1)–(C5) can be reduced to one- or two-dimensional Feynman parameter integrals without difficulty. For example,

$$
\begin{aligned}
J^T_{36} = {}& 2L\int_0^1 dx_1(4b^2 - c) + \frac{3}{16\pi^2}\int_0^1 dx_1 b^2\\
&+ \frac{1}{16\pi^2}\int_0^1 dx_1 \times (4b^2 - c)[-\log\mu^2 + \log(-b^2 + c)]\\
&- \frac{3}{16\pi}\int_0^1 dx_1 b \times (-b^2 + c)^{\frac{1}{2}}\\
&+ \frac{1}{16\pi}\int_0^1 dx_1 b^3(-b^2 + c)^{-\frac{1}{2}} - \frac{1}{8\pi^2}\int_0^1 dx_1 D,
\end{aligned} \tag{C13}
$$

$$
\begin{aligned}
J^T_{45} = {}& 8L\int_0^1 dx_1 b(2b^2 - c) + \frac{1}{4\pi^2}\int_0^1 dx_1 b^3\\
&+ \frac{1}{4\pi^2}\int_0^1 dx_1 \times b(2b^2 - c)[-\log\mu^2 + \log(-b^2 + c)]\\
&+ \frac{1}{16\pi}\int_0^1 dx_1 \times (-b^2 + c)^{\frac{3}{2}} - \frac{3}{8\pi}\int_0^1 dx_1 b^2(-b^2 + c)^{\frac{1}{2}}\\
&+ \frac{1}{16\pi}\int_0^1 dx_1 \times b^4(-b^2 + c)^{-\frac{1}{2}} + \frac{1}{8\pi^2}\int_0^1 dx_1 E,
\end{aligned} \tag{C14}
$$

where

$$
\begin{aligned}
b = {}& (1 - x_1)v\cdot q - \omega,\\
c = {}& (1 - x_1)^2 q^2 - (1 - x_1)q^2 + x_1(m_1^2 - m_2^2) + m_2^2 - i\epsilon,\\
D = {}& \left\{\sqrt{c - b^2}\left[(4b^2 - c)\log\left(1 - \frac{b^2}{c}\right) + 5b^2\right]\right.\\
&\left. + (8b^3 - 6bc)\times\tan^{-1}\left(\frac{b}{\sqrt{c - b^2}}\right)\right\}(2\sqrt{c - b^2})^{-1},\\
E = {}& \left\{b\sqrt{c - b^2}[6(2b^2 - c)(\log(c) - \log[c - b^2]) - 16b^2\right.\\
&\left. + 3c] - 3(8b^4 - 8b^2 c + c^2)\tan^{-1}\left(\frac{b}{\sqrt{c - b^2}}\right)\right\}\\
&\times (3\sqrt{c - b^2})^{-1},
\end{aligned} \tag{C15}
$$

and L is defined in Eq. (A36).

One should notice that in Eqs. (C1)–(C5), if the form of the integral (16) is encountered, the 2PR part must be subtracted using Eq. (17).

However, the evaluations of the above loop integrals are not complete since the kinetic energy terms in the propagators are not included. Here, we further illustrate the calculations considering the kinetic energy terms $\frac{\vec{q}^2}{2M}$. We choose J_0^b as an example,

$$i\int\frac{d^Dl\mu^{4-D}}{(2\pi)^D}\frac{1}{[-v\cdot l-\frac{(\vec{p}-\vec{l})^2}{2M}+\omega+i\varepsilon][l^2-m^2+i\varepsilon]}. \tag{C16}$$

We first apply the Feynman parametrization to Eq. (C16):

$$\begin{aligned}\frac{1}{[-v\cdot l-\frac{(\vec{p}-\vec{l})^2}{2M}+\omega+i\varepsilon][l^2-m^2+i\varepsilon]}&=2\int_0^\infty dy\frac{1}{[l^2-m^2+2y(-v\cdot l-\frac{(\vec{p}-\vec{l})^2}{2M}+\omega)+i\varepsilon]^2}\\&=2\int_0^\infty dy\frac{1}{[l^2-2yv\cdot l+y^2v^2-y^2v^2-\frac{y}{M}(\vec{p}-\vec{l})^2+2y\omega-m^2+i\varepsilon]^2}\\&=2\int_0^\infty dy\frac{1}{[(l-yv)^2-y^2-\frac{y}{M}(\vec{p}-\vec{l})^2+2y\omega-m^2+i\varepsilon]^2}.\end{aligned} \tag{C17}$$

With the substitution $l\to l+yv$ we obtain

$$2\int_0^\infty dy\frac{1}{[l^2-y^2-\frac{y}{M}(\vec{p}-\vec{l})^2+2y\omega-m^2+i\varepsilon]^2}. \tag{C18}$$

Next, we analyze the pole structure of the expression and perform the l_0 integral. We first rewrite the polynomial of l_0 in the denominator:

$$\begin{aligned}&l^2-y^2-\frac{y}{M}(\vec{p}-\vec{l})^2+2y\omega-m^2+i\varepsilon\\&=l_0^2-\vec{l}^2-y^2-\frac{y}{M}(\vec{p}-\vec{l})^2+2y\omega-m^2+i\varepsilon\\&=l_0^2-\left[\vec{l}^2+\frac{y}{M}(\vec{p}-\vec{l})^2+y^2-2y\omega+m^2\right]+i\varepsilon\\&=[l_0+E_l][l_0-E_l],\end{aligned} \tag{C19}$$

where $E_l=\sqrt{\vec{l}^2+\frac{y}{M}(\vec{p}-\vec{l})^2+y^2-2y\omega+m^2}-i\varepsilon$. Therefore, there exist two poles located at $-E_l$ and E_l.

With the expressions above, Eq. (C16) becomes

$$\begin{aligned}&i\int\frac{d^Dl\mu^{4-D}}{(2\pi)^D}\frac{1}{\left[-v\cdot l-\frac{(\vec{p}-\vec{l})^2}{2M}+\omega+i\varepsilon\right][l^2-m^2+i\varepsilon]}\\&=2i\int_0^\infty dy\int\frac{d^Dl\mu^{4-D}}{(2\pi)^D}\frac{1}{[l_0+E_l]^2[l_0-E_l]^2}\\&=2i\int_0^\infty dy\int\frac{d^{D-1}l\mu^{4-D}}{(2\pi)^D}\int dl_0\frac{1}{[l_0+E_l]^2[l_0-E_l]^2}.\end{aligned} \tag{C20}$$

By closing the contour in the upper complex l_0 plane, we obtain the l_0 integral

$$\int dl_0\frac{1}{[l_0+E_l]^2[l_0-E_l]^2}=2\pi i\mathrm{Res}(f(-E_l)), \tag{C21}$$

where $\mathrm{Res}(f(-E_l))$ is the residue at $-E_l$, which can be evaluated by using

$$\mathrm{Res}(f(z_0))=\lim_{z\to z_0}\frac{1}{(m-1)!}\left\{\frac{d^{m-1}}{dz^{m-1}}[(z-z_0)^mf(z)]\right\}, \tag{C22}$$

i.e.,

$$\begin{aligned}&\mathrm{Res}(f(-E_l))\\&=\lim_{l_0\to-E_l}\left\{\frac{d}{dl_0}\left[(l_0-(-E_l))^2\frac{1}{[l_0+E_l]^2[l_0-E_l]^2}\right]\right\}\\&=\lim_{l_0\to-E_l}\frac{2}{(E_l-l_0)^3}\\&=\frac{2}{(2E_l)^3}\\&=\frac{1}{4}\frac{1}{[\vec{l}^2+\frac{y}{M}(\vec{p}-\vec{l})^2+y^2-2y\omega+m^2-i\varepsilon]^{3/2}},\end{aligned} \tag{C23}$$

where the expression $\vec{l}^2+\frac{y}{M}(\vec{p}-\vec{l})^2+y^2-2y\omega+m^2-i\varepsilon$ should be further simplified:

$$\left(1+\frac{y}{M}\right)\left[\vec{l}-\frac{\frac{y}{M}}{1+\frac{y}{M}}\vec{p}\right]^2+\frac{\frac{y}{M}}{1+\frac{y}{M}}\vec{p}^2+(y-\omega)^2+m^2-\omega^2=\left(1+\frac{y}{M}\right)\vec{l}^2+(y-\omega)^2+m^2-\omega^2$$
$$=\left(1+\frac{y}{M}\right)\left[\vec{l}^2+\frac{(y-\omega)^2+m^2-\omega^2}{1+\frac{y}{M}}\right]$$
$$=\left(1+\frac{y}{M}\right)[\vec{l}^2+\Delta] \tag{C24}$$

with

$$\Delta=\frac{(y-\omega)^2+m^2-\omega^2}{1+\frac{y}{M}}. \tag{C25}$$

Then, Eq. (C20) reduces to

$$2i\int_0^\infty dy\int\frac{d^{D-1}l\mu^{4-D}}{(2\pi)^D}(2\pi i)\frac{1}{4}\frac{1}{[(1+\frac{y}{M})[\vec{l}^2+\Delta]]^{3/2}}=-\frac{1}{2}\int_0^\infty dy\int\frac{d^{D-1}l\mu^{4-D}}{(2\pi)^{D-1}}\frac{1}{[(1+\frac{y}{M})[\vec{l}^2+\Delta]]^{3/2}}$$
$$=-\frac{1}{2}\int_0^\infty dy\frac{\mu^{4-D}}{(2\pi)^{\frac{D-1}{2}}}\frac{\Gamma[2-\frac{D}{2}]}{\Gamma[\frac{3}{2}]}\frac{1}{(1+\frac{y}{M})^{3/2}\Delta^{2-\frac{D}{2}}}. \tag{C26}$$

Using

$$y\to y+\omega,\qquad \Delta\to\frac{y^2+m^2-\omega^2}{1+\frac{y+\omega}{M}}, \tag{C27}$$

Eq. (C26) can be further simplified to

$$-\frac{1}{2}\int_{-\omega}^\infty dy\frac{\mu^{4-D}}{(2\pi)^{\frac{D-1}{2}}}\frac{\Gamma[2-\frac{D}{2}]}{\Gamma[\frac{3}{2}]}\frac{1}{(1+\frac{y+\omega}{M})^{3/2}\Delta^{2-\frac{D}{2}}}=-\frac{1}{2}\int_{-\omega}^\infty dy\frac{\mu^\epsilon}{(2\pi)^{\frac{3-\epsilon}{2}}}\frac{\Gamma[\frac{\epsilon}{2}]}{\Gamma[\frac{3}{2}]}\frac{1}{(1+\frac{y+\omega}{M})^{3/2}\Delta^{\frac{\epsilon}{2}}}$$
$$=\frac{-1}{2}\int_0^\infty dy\frac{\mu^\epsilon}{(2\pi)^{\frac{3-\epsilon}{2}}}\frac{\Gamma[\frac{\epsilon}{2}]}{\Gamma[\frac{3}{2}]}\frac{1}{(1+\frac{y+\omega}{M})^{3/2}\Delta^{\frac{\epsilon}{2}}}$$
$$+\frac{-1}{2}\int_{-\omega}^0 dy\frac{\mu^\epsilon}{(2\pi)^{\frac{3-\epsilon}{2}}}\frac{\Gamma[\frac{\epsilon}{2}]}{\Gamma[\frac{3}{2}]}\frac{1}{(1+\frac{y+\omega}{M})^{3/2}\Delta^{\frac{\epsilon}{2}}}, \tag{C28}$$

where $\epsilon=4-D$.

We first discuss the $\int_0^\infty$ part,

$$\frac{-1}{2}\int_0^\infty dy\frac{\mu^\epsilon}{(2\pi)^{\frac{3-\epsilon}{2}}}\frac{\Gamma[\frac{\epsilon}{2}]}{\Gamma[\frac{3}{2}]}\frac{1}{(1+\frac{y+\omega}{M})^{3/2}\Delta^{\frac{\epsilon}{2}}}=\frac{-1}{2}\frac{(4\pi)^{\frac{1}{2}}}{\Gamma[\frac{3}{2}]}\frac{\mu^\epsilon\Gamma[\frac{\epsilon}{2}]}{(4\pi)^{2-\frac{\epsilon}{2}}}\int_0^\infty dy\frac{(1+\frac{y+\omega}{M})^{\frac{-3}{2}}}{\left(\frac{y^2-\omega^2+m^2}{1+\frac{y+\omega}{M}}\right)^{\frac{\epsilon}{2}}}$$
$$=\frac{-1}{2}\frac{(4\pi)^{\frac{1}{2}}}{\Gamma[\frac{3}{2}]}\frac{\mu^\epsilon\Gamma[\frac{\epsilon}{2}]}{(4\pi)^{2-\frac{\epsilon}{2}}}\int_0^\infty dy\frac{(1+\frac{y+\omega}{M})^{\frac{\epsilon-3}{2}}}{(y^2-\omega^2+m^2)^{\frac{\epsilon}{2}}}. \tag{C29}$$

Notice that, if we assume $M\to\infty$, the expression above becomes

$$\frac{-1}{2}\frac{(4\pi)^{\frac{1}{2}}}{\Gamma[\frac{3}{2}]}\frac{\mu^\epsilon\Gamma[\frac{\epsilon}{2}]}{(4\pi)^{2-\frac{\epsilon}{2}}}\int_0^\infty dy\frac{1}{(y^2-\omega^2+m^2)^{\frac{\epsilon}{2}}}=-2\frac{\mu^\epsilon\Gamma[\frac{\epsilon}{2}]}{(4\pi)^{2-\frac{\epsilon}{2}}}\frac{\Gamma[\frac{1}{2}]\Gamma[\frac{-1}{2}]}{2\Gamma[\frac{\epsilon}{2}]}(-\omega^2+m^2)^{\frac{1}{2}-\frac{\epsilon}{2}}$$
$$=\frac{1}{8\pi}(-\omega^2+m^2)^{\frac{1}{2}}. \tag{C30}$$

The result above reproduces part of J_0^b where $\vec{q}^2/M$ in the propagator is not included.

We now discuss the $\int_{-\omega}^{0}$ part:

$$\begin{aligned}\frac{-1}{2}\int_{-\omega}^{0}dy\frac{\mu^{\epsilon}}{(2\pi)^{\frac{3-\epsilon}{2}}}\frac{\Gamma[\frac{\epsilon}{2}]}{\Gamma[\frac{3}{2}]}\frac{1}{(1+\frac{y+\omega}{M})^{3/2}\Delta^{\frac{\epsilon}{2}}}&=\frac{-1}{2}\frac{(4\pi)^{\frac{1}{2}}}{\Gamma[\frac{3}{2}]}\frac{\mu^{\epsilon}\Gamma[\frac{\epsilon}{2}]}{(4\pi)^{2-\frac{\epsilon}{2}}}\int_{-\omega}^{0}dy\frac{(1+\frac{y+\omega}{M})^{\frac{\epsilon-3}{2}}}{(y^2-\omega^2+m^2)^{\frac{\epsilon}{2}}}\\&=-2\left(-2L+\frac{1}{8\pi^2}\log\mu-\frac{1}{16\pi^2}\right)\int_{-\omega}^{0}dy\left(1+\frac{y+\omega}{M}\right)^{\frac{-3}{2}}\times\frac{(1+\frac{y+\omega}{M})^{\frac{\epsilon}{2}}}{(y^2-\omega^2+m^2)^{\frac{\epsilon}{2}}}\\&=-2\left(-2L+\frac{1}{8\pi^2}\log\mu-\frac{1}{16\pi^2}\right)\int_{-\omega}^{0}dy\left(1+\frac{y+\omega}{M}\right)^{\frac{-3}{2}}\times\left[1+\frac{\epsilon}{2}\log\frac{1+\frac{y+\omega}{M}}{y^2-\omega^2+m^2}\right]\\&=\left(4L-\frac{1}{4\pi^2}\log\mu+\frac{1}{8\pi^2}\right)\int_{-\omega}^{0}dy\left(1+\frac{y+\omega}{M}\right)^{\frac{-3}{2}}\\&\quad-\frac{1}{8\pi^2}\int_{-\omega}^{0}dy\left(1+\frac{y+\omega}{M}\right)^{\frac{-3}{2}}\log\frac{1+\frac{y+\omega}{M}}{y^2-\omega^2+m^2},\end{aligned}\tag{C31}$$

where the term containing L [defined in Eq. (A36)] is a divergent part. The expression above will be further evaluated numerically. If we assume $M\to\infty$ again, the result can reproduce another part of J_0^b where $\vec{q}^2/M$ in the propagator is not included at the beginning.

The evaluations of the other loop integrals in Eqs. (C1)–(C5) are similar.

[1] S. Weinberg, Phenomenological Lagrangians, Physica (Amsterdam) **96A**, 327 (1979).
[2] J. Gasser and H. Leutwyler, Chiral perturbation theory to one loop, Ann. Phys. (N.Y.) **158**, 142 (1984).
[3] S. Scherer and M. R. Schindler, *A Primer for Chiral Perturbation Theory* (Springer-Verlag, Berlin, 2012), Vol. 830, p. 1.
[4] E. E. Jenkins and A. V. Manohar, Baryon chiral perturbation theory using a heavy fermion Lagrangian, Phys. Lett. B **255**, 558 (1991).
[5] V. Bernard, N. Kaiser, J. Kambor, and U. G. Meissner, Chiral structure of the nucleon, Nucl. Phys. **B388**, 315 (1992).
[6] V. Bernard, N. Kaiser, and U. G. Meissner, Chiral dynamics in nucleons and nuclei, Int. J. Mod. Phys. E **04**, 193 (1995).
[7] T. Becher and H. Leutwyler, Baryon chiral perturbation theory in manifestly Lorentz invariant form, Eur. Phys. J. C **9**, 643 (1999).
[8] T. Fuchs, J. Gegelia, G. Japaridze, and S. Scherer, Renormalization of relativistic baryon chiral perturbation theory and power counting, Phys. Rev. D **68**, 056005 (2003).
[9] L. Geng, Recent developments in SU(3) covariant baryon chiral perturbation theory, Front. Phys. **8**, 328 (2013).
[10] F. K. Guo, C. Hanhart, and U. G. Meissner, Interactions between heavy mesons and Goldstone bosons from chiral dynamics, Eur. Phys. J. A **40**, 171 (2009).
[11] Y. R. Liu, X. Liu, and S. L. Zhu, Light Pseudoscalar meson and heavy meson scattering lengths, Phys. Rev. D **79**, 094026 (2009).
[12] L. S. Geng, N. Kaiser, J. Martin-Camalich, and W. Weise, Low-energy interactions of Nambu-Goldstone bosons with D mesons in covariant chiral perturbation theory, Phys. Rev. D **82**, 054022 (2010).
[13] P. Wang and X. G. Wang, Study on 0^+ states with open charm in unitarized heavy meson chiral approach, Phys. Rev. D **86**, 014030 (2012).
[14] M. Altenbuchinger, L.-S. Geng, and W. Weise, Scattering lengths of Nambu-Goldstone bosons off D mesons and dynamically generated heavy-light mesons, Phys. Rev. D **89**, 014026 (2014).
[15] Z. H. Guo, U. G. Meiner, and D. L. Yao, New insights into the $D_{s0}^*(2317)$ and other charm scalar mesons, Phys. Rev. D **92**, 094008 (2015).
[16] D. L. Yao, M. L. Du, F. K. Guo, and U. G. Meiner, One-loop analysis of the interactions between charmed mesons and Goldstone bosons, J. High Energy Phys. 11 (2015) 058.
[17] M. L. Du, F. K. Guo, U. G. Meiner, and D. L. Yao, Study of open-charm 0^+ states in unitarized chiral effective theory with one-loop potentials, Eur. Phys. J. C **77**, 728 (2017).
[18] M. L. Du, F. K. Guo, and U. G. Meissner, Subtraction of power counting breaking terms in chiral perturbation theory: Spinless matter fields, J. High Energy Phys. 10 (2016) 122.
[19] S. Weinberg, Nuclear forces from chiral Lagrangians, Phys. Lett. B **251**, 288 (1990).
[20] S. Weinberg, Effective chiral Lagrangians for nucleon—pion interactions and nuclear forces, Nucl. Phys. **B363**, 3 (1991).
[21] C. Ordonez and U. van Kolck, Chiral lagrangians and nuclear forces, Phys. Lett. B **291**, 459 (1992).
[22] C. Ordonez, L. Ray, and U. van Kolck, The two nucleon potential from chiral Lagrangians, Phys. Rev. C **53**, 2086 (1996).

[23] E. Epelbaum, W. Gloeckle, and U. G. Meissner, Nuclear forces from chiral Lagrangians using the method of unitary transformation. 1. Formalism, Nucl. Phys. **A637**, 107 (1998).

[24] E. Epelbaum, W. Gloeckle, and U. G. Meissner, Nuclear forces from chiral Lagrangians using the method of unitary transformation. 2. The two nucleon system, Nucl. Phys. **A671**, 295 (2000).

[25] B. Long and C. J. Yang, Renormalizing chiral nuclear forces: A case study of $^3P_0$, Phys. Rev. C **84**, 057001 (2011).

[26] B. Long and Y. Mei, Cutoff regulators in chiral nuclear effective field theory, Phys. Rev. C **93**, 044003 (2016).

[27] E. Epelbaum, H. Krebs, and U. G. Meiner, Improved chiral nucleon-nucleon potential up to next-to-next-to-next-to-leading order, Eur. Phys. J. A **51**, 53 (2015).

[28] X. W. Kang, J. Haidenbauer, and U. G. Meiner, Antinucleon-nucleon interaction in chiral effective field theory, J. High Energy Phys. 02 (2014) 113.

[29] L. Y. Dai, J. Haidenbauer, and U. G. Meiner, Antinucleon-nucleon interaction at next-to-next-to-next-to-leading order in chiral effective field theory, J. High Energy Phys. 07 (2017) 078.

[30] X. L. Ren, K. W. Li, L. S. Geng, B. W. Long, P. Ring, and J. Meng, Leading order covariant chiral nucleon-nucleon interaction, Chin. Phys. C **42**, 014103 (2018).

[31] E. Epelbaum, H. W. Hammer, and U. G. Meissner, Modern theory of nuclear forces, Rev. Mod. Phys. **81**, 1773 (2009).

[32] R. Machleidt and D. R. Entem, Chiral effective field theory and nuclear forces, Phys. Rep. **503**, 1 (2011).

[33] M. P. Valderrama, Perturbative renormalizability of chiral two pion exchange in nucleon-nucleon scattering, Phys. Rev. C **83**, 024003 (2011).

[34] M. P. Valderrama, Perturbative renormalizability of chiral two pion exchange in nucleon-nucleon scattering: P- and D-waves, Phys. Rev. C **84**, 064002 (2011).

[35] B. Long and C. J. Yang, Short-range nuclear forces in singlet channels, Phys. Rev. C **86**, 024001 (2012).

[36] U. G. Meissner, The long and winding road from chiral effective Lagrangians to nuclear structure, Phys. Scr. **91**, 033005 (2016).

[37] H. X. Chen, W. Chen, X. Liu, and S. L. Zhu, The hidden-charm pentaquark and tetraquark states, Phys. Rep. **639**, 1 (2016).

[38] S. K. Choi *et al.* (Belle Collaboration), Observation of a Narrow Charmonium-Like State in Exclusive $B^{+(-)} \to K^{+(-)}\pi^+\pi^- J/\psi$ Decays, Phys. Rev. Lett. **91**, 262001 (2003).

[39] S. Godfrey and N. Isgur, Mesons in a relativized quark model with chromodynamics, Phys. Rev. D **32**, 189 (1985).

[40] R. Aaij *et al.* (LHCb Collaboration), Observation of $J/\psi p$ Resonances Consistent with Pentaquark States in $\Lambda_b^0 \to J/\psi K^- p$ Decays, Phys. Rev. Lett. **115**, 072001 (2015).

[41] V. M. Abazov *et al.* (D0 Collaboration), Evidence for a $B_s^0\pi^\pm$ State, Phys. Rev. Lett. **117**, 022003 (2016).

[42] R. Molina and E. Oset, The $Y(3940)$, $Z(3930)$ and the $X(4160)$ as dynamically generated resonances from the vector-vector interaction, Phys. Rev. D **80**, 114013 (2009).

[43] F. Aceti, M. Bayar, E. Oset, A. Martinez Torres, K. P. Khemchandani, J. M. Dias, F. S. Navarra, and M. Nielsen, Prediction of an $I = 1$ $D\bar{D}^*$ state and relationship to the claimed $Z_c(3900)$, $Z_c(3885)$, Phys. Rev. D **90**, 016003 (2014).

[44] J. He, The $Z_c(3900)$ as a resonance from the $D\bar{D}^*$ interaction, Phys. Rev. D **92**, 034004 (2015).

[45] Q. R. Gong, Z. H. Guo, C. Meng, G. Y. Tang, Y. F. Wang, and H. Q. Zheng, $Z_c(3900)$ as a $D\bar{D}^*$ molecule from the pole counting rule, Phys. Rev. D **94**, 114019 (2016).

[46] Y. C. Yang, Z. Y. Tan, J. Ping, and H. S. Zong, Possible $D^{(*)}\bar{D}^{(*)}$ and $B^{(*)}\bar{B}^{(*)}$ molecular states in the extended constituent quark models, Eur. Phys. J. C **77**, 575 (2017).

[47] M. T. AlFiky, F. Gabbiani, and A. A. Petrov, $X(3872)$: Hadronic molecules in effective field theory, Phys. Lett. B **640**, 238 (2006).

[48] S. Fleming, M. Kusunoki, T. Mehen, and U. van Kolck, Pion interactions in the $X(3872)$, Phys. Rev. D **76**, 034006 (2007).

[49] S. Fleming and T. Mehen, Hadronic decays of the $X(3872)$ to chi(cJ) in effective field theory, Phys. Rev. D **78**, 094019 (2008).

[50] V. Baru, A. A. Filin, C. Hanhart, Y. S. Kalashnikova, A. E. Kudryavtsev, and A. V. Nefediev, Three-body $D\bar{D}\pi$ dynamics for the $X(3872)$, Phys. Rev. D **84**, 074029 (2011).

[51] M. P. Valderrama, Power counting and perturbative one pion exchange in heavy meson molecules, Phys. Rev. D **85**, 114037 (2012).

[52] J. Nieves and M. P. Valderrama, The heavy quark spin symmetry partners of the $X(3872)$, Phys. Rev. D **86**, 056004 (2012).

[53] C. Meng, J. J. Sanz-Cillero, M. Shi, D. L. Yao, and H. Q. Zheng, Refined analysis on the $X(3872)$ resonance, Phys. Rev. D **92**, 034020 (2015).

[54] V. Baru, E. Epelbaum, A. A. Filin, J. Gegelia, and A. V. Nefediev, Binding energy of the $X(3872)$ at unphysical pion masses, Phys. Rev. D **92**, 114016 (2015).

[55] V. Baru, E. Epelbaum, A. A. Filin, F.-K. Guo, H.-W. Hammer, C. Hanhart, U.-G. Meiner, and A. V. Nefediev, Remarks on study of $X(3872)$ from effective field theory with pion-exchange interaction, Phys. Rev. D **91**, 034002 (2015).

[56] M. Jansen, H.-W. Hammer, and Y. Jia, Finite volume corrections to the binding energy of the $X(3872)$, Phys. Rev. D **92**, 114031 (2015).

[57] E. Braaten, Galilean-invariant effective field theory for the $X(3872)$, Phys. Rev. D **91**, 114007 (2015).

[58] V. Baru, E. Epelbaum, A. A. Filin, C. Hanhart, U. G. Meissner, and A. V. Nefediev, Heavy-quark spin symmetry partners of the X (3872) revisited, Phys. Lett. B **763**, 20 (2016).

[59] F. K. Guo, C. Hanhart, U. G. Meiner, Q. Wang, Q. Zhao, and B. S. Zou, Hadronic molecules, Rev. Mod. Phys. **90**, 015004 (2018).

[60] Y. R. Liu, X. Liu, W. Z. Deng, and S. L. Zhu, Is $X(3872)$ really a molecular state?, Eur. Phys. J. C **56**, 63 (2008).

[61] X. Liu, Z. G. Luo, Y. R. Liu, and S. L. Zhu, $X(3872)$ and other possible heavy molecular states, Eur. Phys. J. C **61**, 411 (2009).

[62] I. W. Lee, A. Faessler, T. Gutsche, and V. E. Lyubovitskij, $X(3872)$ as a molecular DD^* state in a potential model, Phys. Rev. D **80**, 094005 (2009).

[63] N. Li and S. L. Zhu, Isospin breaking, coupled-channel effects and diagnosis of $X(3872)$, Phys. Rev. D **86**, 074022 (2012).

[64] E. Epelbaum, U. G. Meissner, W. Gloeckle, and C. Elster, Resonance saturation for four nucleon operators, Phys. Rev. C **65**, 044001 (2002).

[65] M. Mattson *et al.* (SELEX Collaboration), First observation of the doubly charmed baryon Ξ_{cc}^+, Phys. Rev. Lett. **89**, 112001 (2002).

[66] Z. F. Sun, Z. W. Liu, X. Liu, and S. L. Zhu, Masses and axial currents of the doubly charmed baryons, Phys. Rev. D **91**, 094030 (2015).

[67] J. Hu and T. Mehen, Chiral Lagrangian with heavy quark-diquark symmetry, Phys. Rev. D **73**, 054003 (2006).

[68] F. S. Yu, H. Y. Jiang, R. H. Li, C. D. L, W. Wang, and Z. X. Zhao, Discovery potentials of doubly charmed baryons, Chin. Phys. C **42**, 051001 (2018).

[69] H. X. Chen, W. Chen, X. Liu, Y. R. Liu, and S. L. Zhu, A review of the open charm and open bottom systems, Rep. Prog. Phys. **80**, 076201 (2017).

[70] H. X. Chen, Q. Mao, W. Chen, X. Liu, and S. L. Zhu, Establishing low-lying doubly charmed baryons, Phys. Rev. D **96**, 031501 (2017).

[71] H. S. Li, L. Meng, Z. W. Liu, and S. L. Zhu, Magnetic moments of the doubly charmed and bottomed baryons, Phys. Rev. D **96**, 076011 (2017).

[72] W. Wang, Z. P. Xing, and J. Xu, Weak Decays of doubly heavy baryons: SU(3) analysis, Eur. Phys. J. C **77**, 800 (2017).

[73] M. Karliner and J. L. Rosner, Quark-level analogue of nuclear fusion with doubly-heavy baryons, Nature (London) **551**, 89 (2017).

[74] R. Aaij *et al.* (LHCb Collaboration), Observation of the doubly charmed baryon Ξ_{cc}^{++}, Phys. Rev. Lett. **119**, 112001 (2017).

[75] S. Ohkoda, Y. Yamaguchi, S. Yasui, K. Sudoh, and A. Hosaka, Exotic mesons with double charm and bottom flavor, Phys. Rev. D **86**, 034019 (2012).

[76] N. Li, Z. F. Sun, X. Liu, and S. L. Zhu, Coupled-channel analysis of the possible $D^{(*)}D^{(*)}$, $\bar{B}^{(*)}\bar{B}^{(*)}$ and $D^{(*)}\bar{B}^{(*)}$ molecular states, Phys. Rev. D **88**, 114008 (2013).

[77] L. M. Abreu, Hadronic states with both open charm and bottom in effective field theory, Nucl. Phys. **A940**, 1 (2015).

[78] S. Sakai, L. Roca, and E. Oset, Charm-beauty meson bound states from $B(B^*)D(D^*)$ and $B(B^*)\bar{D}(\bar{D}^*)$ interaction, Phys. Rev. D **96**, 054023 (2017).

[79] W. Detmold, K. Orginos, and M. J. Savage, BB potentials in quenched lattice QCD, Phys. Rev. D **76**, 114503 (2007).

[80] P. Bicudo, K. Cichy, A. Peters, and M. Wagner, BB interactions with static bottom quarks from Lattice QCD, Phys. Rev. D **93**, 034501 (2016).

[81] A. Francis, R. J. Hudspith, R. Lewis, and K. Maltman, Lattice Prediction for Deeply Bound Doubly Heavy Tetraquarks, Phys. Rev. Lett. **118**, 142001 (2017).

[82] Z. W. Liu, N. Li, and S. L. Zhu, Chiral perturbation theory and the $\bar{B}\bar{B}$ strong interaction, Phys. Rev. D **89**, 074015 (2014).

[83] G. Burdman and J. F. Donoghue, Union of chiral and heavy quark symmetries, Phys. Lett. B **280**, 287 (1992).

[84] M. B. Wise, Chiral perturbation theory for hadrons containing a heavy quark, Phys. Rev. D **45**, R2188 (1992).

[85] T. M. Yan, H. Y. Cheng, C. Y. Cheung, G. L. Lin, Y. C. Lin, and H. L. Yu, Heavy quark symmetry and chiral dynamics, Phys. Rev. D **46**, 1148 (1992); Erratum, Phys. Rev. D **55**, 5851(E) (1997).

[86] Z. F. Sun, J. He, X. Liu, Z. G. Luo, and S. L. Zhu, $Z_b(10610)^{\pm}$ and $Z_b(10650)^{\pm}$ as the $B^*\bar{B}$ and $B^*\bar{B}^*$ molecular states, Phys. Rev. D **84**, 054002 (2011).

[87] Z. F. Sun, Z. G. Luo, J. He, X. Liu, and S. L. Zhu, A note on the $B^*\bar{B}$, $B^*\bar{B}^*$, $D^*\bar{D}$, $D^*\bar{D}^*$, molecular states, Chin. Phys. C **36**, 194 (2012).

[88] S. L. Zhu, C. M. Maekawa, B. R. Holstein, M. J. Ramsey-Musolf, and U. van Kolck, Nuclear parity-violation in effective field theory, Nucl. Phys. **A748**, 435 (2005).

[89] D. Gülmez, U.-G. Meißner, and J. A. Oller, A chiral covariant approach to $\rho\rho$ scattering, Eur. Phys. J. C **77**, 460 (2017).

[90] A. Abada, D. Becirevic, P. Boucaud, G. Herdoiza, J. P. Leroy, A. Le Yaouanc, O. Pene, and J. Rodriguez-Quintero, First lattice QCD estimate of the $g_{D^*D\pi}$ coupling, Phys. Rev. D **66**, 074504 (2002).

[91] D. Becirevic and F. Sanfilippo, Theoretical estimate of the $D^* \to D\pi$ decay rate, Phys. Lett. B **721**, 94 (2013).

[92] K. U. Can, G. Erkol, M. Oka, A. Ozpineci, and T. T. Takahashi, Vector and axial-vector couplings of D and D^* mesons in $2+1$ flavor Lattice QCD, Phys. Lett. B **719**, 103 (2013).

[93] P. Colangelo, G. Nardulli, A. Deandrea, N. Di Bartolomeo, R. Gatto, and F. Feruglio, On the coupling of heavy mesons to pions in QCD, Phys. Lett. B **339**, 151 (1994).

[94] V. M. Belyaev, V. M. Braun, A. Khodjamirian, and R. Ruckl, $D^*D\pi$ and $B^*B\pi$ couplings in QCD, Phys. Rev. D **51**, 6177 (1995).

[95] H. G. Dosch and S. Narison, $B^*B\pi$ couplings and $D^* \to D\pi$ decays within a $1/M$ expansion in full QCD, Phys. Lett. B **368**, 163 (1996).

[96] P. Colangelo and F. De Fazio, QCD interactions of heavy mesons with pions by light cone sum rules, Eur. Phys. J. C **4**, 503 (1998).

[97] M. E. Bracco, M. Chiapparini, F. S. Navarra, and M. Nielsen, Charm couplings and form factors in QCD sum rules, Prog. Part. Nucl. Phys. **67**, 1019 (2012).

[98] P. Colangelo, F. De Fazio, and G. Nardulli, D^* radiative decays and strong coupling of heavy mesons with soft pions in a QCD relativistic potential model, Phys. Lett. B **334**, 175 (1994).

[99] D. Becirevic and A. Le Yaouanc, G coupling ($g_{B^*B\pi}$, $g_{D^*D\pi}$): A Quark model with Dirac equation, J. High Energy Phys. 03 (1999) 021.

[100] B. El-Bennich, M. A. Ivanov, and C. D. Roberts, Strong $D^* \to D\pi$ and $B^* \to B\pi$ couplings, Phys. Rev. C **83**, 025205 (2011).

[101] C. Patrignani *et al.* (Particle Data Group), Review of particle physics, Chin. Phys. C **40**, 100001 (2016).
[102] G. Ecker, J. Gasser, A. Pich, and E. de Rafael, The role of resonances in chiral perturbation theory, Nucl. Phys. **B321**, 311 (1989).
[103] J. F. Donoghue, C. Ramirez, and G. Valencia, The spectrum of QCD and Chiral Lagrangians of the strong and weak interactions, Phys. Rev. D **39**, 1947 (1989).
[104] V. Bernard, N. Kaiser, and U. G. Meissner, Aspects of chiral pion—nucleon physics, Nucl. Phys. **A615**, 483 (1997).
[105] M. L. Du, F. K. Guo, U. G. Meissner, and D. L. Yao, Aspects of the low-energy constants in the chiral Lagrangian for charmed mesons, Phys. Rev. D **94**, 094037 (2016).
[106] J. X. Lu, L. S. Geng, and M. P. Valderrama, Heavy baryon molecules in effective field theory, arXiv:1706.02588.
[107] W. A. Bardeen, E. J. Eichten, and C. T. Hill, Chiral multiplets of heavy—light mesons, Phys. Rev. D **68**, 054024 (2003).
[108] D. B. Kaplan, M. J. Savage, and M. B. Wise, A new expansion for nucleon-nucleon interactions, Phys. Lett. B **424**, 390 (1998).
[109] J. Nieves, Renormalization of the one pion exchange NN interaction in presence of derivative contact interactions, Phys. Lett. B **568**, 109 (2003).
[110] J. F. Yang and J. H. Huang, Renormalization of NN scattering: Contact potential, Phys. Rev. C **71**, 034001 (2005).
[111] M. P. Valderrama and E. Ruiz Arriola, Renormalization of the NN interaction with a chiral two-pion-exchange potential: Central phases and the deuteron, Phys. Rev. C **74**, 054001 (2006).
[112] M. P. Valderrama and E. Ruiz Arriola, Renormalization of NN interaction with chiral two pion exchange potential: Non-central phases, Phys. Rev. C **74**, 064004 (2006); Phys. Rev. C **75**, 059905(E) (2007).
[113] M. P. Valderrama, Power counting and Wilsonian renormalization in nuclear effective field theory, Int. J. Mod. Phys. E **25**, 1641007 (2016).
[114] B. Aubert *et al.* (*BABAR* Collaboration), Search for doubly charmed baryons Ξ_{cc}^{+} and Ξ_{cc}^{++} in *BABAR*, Phys. Rev. D **74**, 011103 (2006).
[115] R. Aaij *et al.* (LHCb Collaboration), Search for the doubly charmed baryon Ξ_{cc}^{+}, J. High Energy Phys. 12 (2013) 090.